



Contents lists available at ScienceDirect

Remote Sensing of Environment

journal homepage: www.elsevier.com/locate/rse

Historical background and current developments for mapping burned area from satellite Earth observation



Emilio Chuvieco^{a,*}, Florent Mouillot^b, Guido R. van der Werf^c, Jesús San Miguel^d, Mihai Tanase^a, Nikos Koutsias^e, Mariano García^a, Marta Yebra^f, Marc Padilla^g, Ioannis Gitas^h, Angelika Heilⁱ, Todd J. Hawbaker^j, Louis Giglio^k

^a Environmental Remote Sensing Research Group, Department of Geology, Geography and the Environment, Universidad de Alcalá, Calle Colegios 2, Alcalá de Henares 28801, Spain

^b IRD, UMR CEFE 5175, Centre National de la Recherche Scientifique (CNRS), Université de Montpellier, Université Paul-Valéry Montpellier, Ecole pratique des hautes études (EPHE), Institut de Recherche pour le Développement (IRD), 1919 route de Mende, 34293 Montpellier cedex 5, France

^c Department of Earth Sciences, Faculty of Science, Vrije Universiteit Amsterdam, De Boelelaan 1085, 1081HV Amsterdam, the Netherlands

^d European Commission Joint Research Centre, Directorate E – Space, Security and Migration, Via Fermi 2749, Ispra I-21027, Italy

^e Department of Environmental and Natural Resources Management, University of Patras, G. Seferi 2, Agrinio GR-30100, Greece

^f Fenner School of Environment and Society, The Australian National University, Acton, ACT, Australia, and Bushfire, Natural Hazards Cooperative Research Centre, Melbourne, Australia

^g Centre for Landscape & Climate Research, Leicester Institute for Space and Earth Observation, School of Geography, University of Leicester, Leicester LE1 7RH, United Kingdom

^h Laboratory of Forest Management and Remote Sensing, School of Forestry and Natural Environment, Aristotle University of Thessaloniki, Moschounti 59, Thessaloniki GR-54124, Greece

ⁱ Max Planck Institute for Meteorology, Environmental Modeling, Hamburg, Germany

^j U.S. Geological Survey, Geosciences and Environmental Change Science Center, Denver, CO 80225, USA

^k Department of Geographical Sciences, University of Maryland, College Park, MD, USA

ARTICLE INFO

Keywords:

Burned area
Fire
Fire impacts
Lidar
Radar
Climate change

ABSTRACT

Fire has a diverse range of impacts on Earth's physical and social systems. Accurate and up to date information on areas affected by fire is critical to better understand drivers of fire activity, as well as its relevance for biogeochemical cycles, climate, air quality, and to aid fire management. Mapping burned areas was traditionally done from field sketches. With the launch of the first Earth observation satellites, remote sensing quickly became a more practical alternative to detect burned areas, as they provide timely regional and global coverage of fire occurrence. This review paper explores the physical basis to detect burned area from satellite observations, describes the historical trends of using satellite sensors to monitor burned areas, summarizes the most recent approaches to map burned areas and evaluates the existing burned area products (both at global and regional scales). Finally, it identifies potential future opportunities to further improve burned area detection from Earth observation satellites.

1. Introduction: impacts of biomass burning

Fire is a natural disturbance agent in many ecosystems, helping to promote diversity and natural regeneration (Kelly and Brotons, 2017). However, fire has also been used since the beginning of human history as a tool for hunting, land management and deforestation (Pyne, 1995). Fire cycles were historically associated with climate oscillations, particularly with temperature increases in boreal and temperate regions (Marlon et al., 2013), and with multimillennial-scale changes in precipitation amount and timing in tropical regions (Daniau et al., 2013).

However, in the last centuries, human factors have taken pre-dominance, either as a source of ignition or as a force of fire suppression, especially in developed countries. These alterations of natural fire regimes can have negative impacts on biodiversity, forest structure and resilience, particularly in equatorial regions where evergreen forests have become vulnerable to fire (Gilroy et al., 2014; Lewis et al., 2015).

Biomass burning is widely recognized as one of the critical factors affecting atmospheric chemistry, as a significant share of aerosols and greenhouse gas emissions are produced from burning (Knorr et al., 2016; van der Werf et al., 2010). Fires also affect carbon budgets

* Corresponding author.

E-mail address: emilio.chuvieco@uah.es (E. Chuvieco).

<https://doi.org/10.1016/j.rse.2019.02.013>

Received 17 November 2018; Received in revised form 14 February 2019; Accepted 16 February 2019

Available online 05 March 2019

0034-4257/ © 2019 The Authors. Published by Elsevier Inc. This is an open access article under the CC BY-NC-ND license (<http://creativecommons.org/licenses/by-nc-nd/4.0/>).

(Thonicke et al., 2010; Yue et al., 2015) and vegetation succession (Bowman et al., 2009), and remain a significant driver of land use transformation (Lewis et al., 2015). In densely populated areas, the impacts of fires on air quality and associated health impacts may be very important, particularly for people with respiratory problems and heart diseases and children (Reid et al., 2016). Emissions from forest fires in critical years, such as the “El Niño” events in Indonesia in 1997 and 2015 (with impacts on transboundary air pollution) or the fires in Russia in 2010, resulted in substantial health impacts (Cascio, 2018; Koplitz et al., 2016; Hu et al., 2018; Page et al., 2002).

At regional and local scales, fires have important socio-economic implications as well, both affecting lives and property (Chuvieco et al., 2010). Catastrophic seasons (with many human casualties) have been witnessed in recent years, mainly associated with heat waves and droughts (Bowman et al., 2017): Greece, 2007 and 2018; Australia, 2009; Russia, 2010; USA, 2013, 2017 and 2018; Canada, 2016; Chile, 2017; and Portugal, 2003, 2005 and 2017, among others. Fire also affects soil erosion and the hydrological cycle (Doerr et al., 2006). The wide variety of fire effects suggests a need for comprehensive evaluations of fire vulnerability (Chuvieco et al., 2014; McWethy et al., 2013), which includes the analysis of potential damages of fires on societal and ecological values, as well as integrating those losses throughout time considering regeneration intervals (Rodrigues et al. 2014).

There is still much uncertainty in the area affected by biomass burning worldwide (including forest fires, savanna and cropland burnings). Recent assessments based on Earth observation (EO) satellites estimate that around 4 million km² are burned globally every year (Chuvieco et al., 2018; Giglio et al., 2018). This area is approximately equivalent to the size of India and Pakistan combined. This estimate is based on coarse resolution sensors (with pixels larger than 250 m), and is likely to be a conservative estimate of total burned area (BA), since most analyses comparing global with regional products have found that they underestimate actual BA (Hall et al., 2016; Hawbaker et al., 2017; Mangeon et al., 2016). In fact, a recent BA product covering Africa with Sentinel-2 images for a single year estimates 1.8 times more BA than the estimates derived from the Moderate Resolution Imaging Spectroradiometer (MODIS) products. This high discrepancy is mostly caused by small fires (<100 ha) (Roteta et al., 2019). Future studies with even higher resolution sensors (Whittier and Gray, 2016) may further increase estimates of global BA.

Most burning occurs in areas with a marked dry season, mostly savannas and their transitional zone to tropical rainforests, Mediterranean forests, Central Asian grasslands, and boreal forests of Asia and America (Chuvieco et al., 2016; Giglio et al., 2013). Even though the recent trends in global BA indicate a decrease in fire-affected areas due to agricultural expansion in regions with low tree cover (Andela et al., 2017), the impacts of fire in forested and even tundra regions are expected to increase in the future due to climate and societal changes (Jolly et al., 2015; Roos et al., 2016). Therefore, it is particularly relevant to improve our knowledge of drivers behind fire occurrence and fire impacts to alleviate current and foreseen future effects of biomass burning (Forkel et al., 2019; Hantson et al., 2016). For doing so, a better description is needed of the spatial-temporal patterns of biomass burning.

Historically, government agencies collected BA information from ground estimates, based on reports from fire management teams (Mouillot and Field, 2005). The differences in the methods used by individual countries and the discontinuity in data collection by government agencies throughout the years make these sources unreliable when analyses are performed at regional, continental or global scales. Satellite imagery has been used for BA detection as a sound alternative for compiling reliable information on fire-affected areas since the beginning of satellite observations. Less than two years after the launch of the first Landsat satellite in 1972 (then Earth Resources Technology Satellite 1 or ERTS-1), a conference paper was presented using satellite data for BA mapping (Hitchcock and Hoffer, 1974). Since then, the use

of satellite imagery for BA detection and mapping has been addressed in many peer-reviewed journals, book chapters, and conference proceedings. This review paper aims to evaluate the historical developments of satellite-based studies on BA estimation, the different sensors and methods that have been used, and the strengths and limitations of current available BA products, with particular emphasis on global datasets. We focus on BA mapping, assuming a binary detection (burned/unburned). Analysis of fire effects or regeneration after fire has been covered elsewhere (Chu and Guo, 2014; Storey et al., 2016; Veraverbeke and Hook, 2013).

This review is organized around several sections. First, the requirements of BA information by different user communities is covered, with particular emphasis on atmospheric emissions and dynamic global vegetation models. Then a brief section describes the spectral characteristics of fire-affected areas, which are the basis of retrieving BA information from satellite sensors. Then, a historical analysis presents the trends in BA mapping since the early 1980s until the beginning of this century. Next, the current state of the art and expected evolution are appraised, distinguishing in both cases sensors and methodological approaches. The last section briefly summarizes existing BA products, their main strengths and limitations and provides an overview of the main challenges ahead for retrieving BA from satellite imagery. A list of acronyms is included at the annex to help readers with the different products, missions and agencies involved.

2. Needs and uses of burned area information

Most global BA products initially aimed at fulfilling the needs of climate modelers, as fire disturbance is considered one of the Essential Climate Variables (GCOS, 2016), but increasing accuracy and systematic delivery at global scale lead to civil protection services, environmental and forest protection services, insurance companies and health planners, among other communities to increasingly use these data as a surrogate to the lack of local information as reviewed in Mouillot et al. (2014). The need of BA information and effects of forest fires at the global scale are also relevant to address international initiatives and commitments related to fire emissions, such as the Kyoto Protocol and the agreements at the United National Conference on Climate Change in Paris (COP21), or the United Nations Sendai Framework on Disaster Risk Reduction 2015–2030, through the monitoring of progress in the Sustainable Development Goals (SDGs), for which global information on fire effects is a key variable. These communities may have different needs and therefore, the BA products need to be optimized for a wide range of end-user requirements.

The emergence of new global satellite records catalyzed substantial progress in fire emissions estimation over the past three decades. The first global estimates of biomass burning emissions relied on biome-aggregated best-guess values of the average annual area burned, combined with biome-averaged estimates of biomass density and burning efficiency (Seiler and Crutzen, 1980). Subsequent efforts used vegetation and land use maps to spatially disaggregate the annual average emission estimates to 5° (Müller, 1992; Hao and Liu, 1994) and later to 1° (Lobert et al., 1999) spatial resolution. They were based on yearly national fire statistics and other proxies (Mouillot et al., 2006). By the early 2000s, the integration of satellite observations allowed for a better representation of the spatial and temporal variability of fire emissions (Duncan et al., 2003; Ito and Penner, 2004) that relied on the first available global BA maps computed from satellite information of post-fire reflectance: the GBA2000 product (Grégoire et al., 2003) and GLOBSCAR (Simon et al., 2004). The first version of the Global Fire Emission Database (GFED) then provided 1° × 1° gridded monthly fire emissions from 1997 to 2002 (van der Werf et al., 2003, 2004). GFED uses gridded 0.5° or 0.25° BA data in a biogeochemical model where available biomass to burn in vegetation and soil is determined by coarse scale land cover types, soil types and their corresponding water holding capacity and climate (CASA). However, bias may be introduced when

emissions are simulated at coarse resolution as fires may be highly selective so that some places might have high fire frequency while other places may never burn (Barros and Pereira, 2014; Scholz et al. 2014). Therefore, regional studies using fine resolution datasets are preferred (Veraverbeke et al., 2015; Yospin et al., 2015).

Mid-resolution global remote sensing datasets recently provided additional information on the distribution of fire within coarse resolution grid cells to estimate reburning rates and vegetation types or forest age cohorts affected by fires. In GFED version 2, fire emissions estimates relied on BA time series that were established by calibrating HS to the first and, at that time, only regionally available direct BA maps from the MODIS sensor (Giglio et al., 2006; van der Werf et al., 2006). In the following GFED releases (GFED3, GFED4s) (van der Werf et al., 2010; van der Werf et al., 2017), the monthly emission estimates mainly relied on directly mapped MODIS BA (Giglio et al., 2006; Giglio et al., 2010). The product's spatial resolution increased to 0.25° and HS-based gridded scalars were added allowing for estimation of daily and 3-hourly emission fluxes (Mu et al., 2011). In GFED4s (van der Werf et al., 2017), HS were additionally used to estimate emissions from small fires that are unresolved by MODIS imagery.

Three-dimensional chemical transport models (CTMs) have used these global BA-derived fire emissions (Matthias et al., 2018) in addition to prescribed meteorological fields as input to determine atmospheric composition, both as retrospective analyses and as forecasts. Most CTM applications require high spatial and temporal resolution, and temporal accuracy of fire emissions usually provided by GFED (Strode et al., 2016). Additionally, near real time (NRT) CTM systems require more prompt data availability. Fire emission inventories developed to address this last requirement alternatively rely on satellite observations of HS or of their radiant heat released (fire radiative power: FRP) (Wiedinmyer et al., 2011). Chemistry climate models (CCMs) investigate the interactions between climate and atmospheric chemistry on decadal to centennial scales (Isaksen et al., 2009). While CCMs simulate the physical characteristics of the climate system, state-of-the-art global CCM applications such as those supporting the Intergovernmental Panel on Climate Change (IPCC) Assessment Reports (AR) use prescribed anthropogenic and biomass burning emissions as boundary conditions (Lamarque et al., 2013). These applications require low spatial and temporal resolution but long-term emission inventories (much longer than available remotely sensed BA time series) with high temporal stability in accuracy so that long-term effects of fires on tree age cohorts and their impact on carbon budget are taken into account (Yue et al., 2014). Such inventories rely on national statistics, historical regional remote sensing BA estimates and storylines (Mouillot and Field, 2005; Mouillot et al., 2006; Mievile et al., 2010), or the global charcoal database and fire models embedded in dynamic vegetation models (DGVMs) (van Marle et al., 2017).

Beside direct aerosol emission from biomass burning, the climate system is also linked to the terrestrial global carbon budget affected by fires through the combustion of live and dead biomass and soil litter and the subsequent post-fire changes in vegetation and surface fluxes. Dynamic global vegetation models including fire modules can reconstruct and project BA under changing climate, atmospheric CO₂ concentration and land use change. Processes are identified from global BA data (Bistinas et al., 2014) and simulated BA are benchmarked with available BA data (cf. Hantson et al., 2016 for review). Fire modules embedded in DGVMs aim at dynamically simulating historical and future biosphere/atm interactions accounting for the seasonal burned BA across global biomes based on fire weather and available fuel biomass and water status derived from a process-based dynamic vegetation model (Hantson et al., 2016).

With the increasing availability of moderate resolution data, fire patches, generated from 250 to 500 m resolution sensors have been recently part of global BA product assessments (Chuvieco et al., 2016; Nogueira et al., 2017). They can be generated by aggregating neighboring pixels with near-similar burn-dates (Archibald et al., 2009;

Hantson et al., 2015). Fire patch size, complexity, and unburned islands also influence tree species colonization rates from seed dispersal (Meddens et al., 2018), affecting subsequent carbon sequestration dynamics (Duncan and Duncan, 2000; Caughlin et al., 2016). Laurent et al. (2018) estimated patch complexity, elongation and rate of spread from a global 250-m BA dataset, to estimate proxies on fire spreading processes to improve fire modules within DGVMs.

Beside these main topics for which global BA was initially developed, BA information is also essential for legal purposes at local to regional scales as for proper cadastral recording of fire effects, regarding land use and insurance costs or illegal burning (Mouillot et al., 2014 for review). For instance, in Europe, most countries have issued laws by which the land use of fire-affected areas cannot be changed for 10 to 30 years, depending on the country. Insurance premium and insurance costs require detailed information of areas affected by fires and the level of fire severity, as well as post fire hazards such as landslides or mudflows after fires. Therefore, reliable BA information is required by the country and the European Union for the assessment of economic losses caused by the fires. Funds associated with the planning of remediation and revegetation efforts after fires are based on the maps of BA and the assessment of economic losses. For instance, the European Union Solidarity Fund (EUSF) is provided to countries that suffered damages by fires above a given threshold of its global domestic product (GDP). The use of the EUSF is currently a common practice, which is applied after the catastrophic fires, e.g. Portugal (2003, 2005, 2017), Spain (2003, 2012, 2017), and Greece (2007, 2018). Fire managers and ecologists rely on BA information as well, to better assess fire risk and implement risk reduction measures, and to improve fire history characterization, particularly on fuel loads (typically using fuel accumulations curves: Birk and Simpson, 1980).

International cooperation was necessary to establish services such as the International Charter Space and Major Disasters and the Copernicus Emergency Management Services Mapping, which aim at the rapid acquisition of satellite imagery and the immediate mapping of effects of catastrophic fires, among other disasters. The need of BA information and effects of forest fires at the global scale is also relevant to address international initiatives and commitments related to fire emissions, such as the Kyoto Protocol and the agreements at the COP21 UN Conference on Climate Change in Paris, or the United Nations Sendai Framework on Disaster Risk Reduction 2015–2030, through the monitoring of progress in the Sustainable Development Goals (SDGs), for which global information on fire effects is a key variable.

3. Physical basis for Earth observation of burned areas

Fire impacts on vegetation are not binary (burned/unburned), but rather they have a wide variety of conditions, depending on the type of fire, fire behavior, and the time between fire extinction and image acquisition. Therefore, the post-fire signal as well as its changes from pre-fire reflectance, temperature or backscatter may be very diverse. Thus, the analysis of both post-fire and temporal changes in spectral behavior provides relevant information to understand fire impacts, while monitoring post-fire changes throughout time helps to understand regeneration patterns.

The type of fire relates to the vegetation strata affected by the burning: whether fire impacts the surface fuels and understory component of the forest cover (surface fire), the canopy (crown fire), or even just the in-depth soil layer (underground fire). Wherever the tree cover is dense, surface fires are difficult to detect from remote sensing measurements (Pereira et al., 2004). This is particularly challenging for tropical fires, which tend to have moderate severity but important impacts when they are recurrent (Cochrane et al., 1999). Crown fires are easier to detect, while underground fires may only be detected by thermal sensors, as vegetation reflectance changes after the root system is affected by the intense heat (Fig. 1).

Fire behavior affects the heat released and the propagation speed of

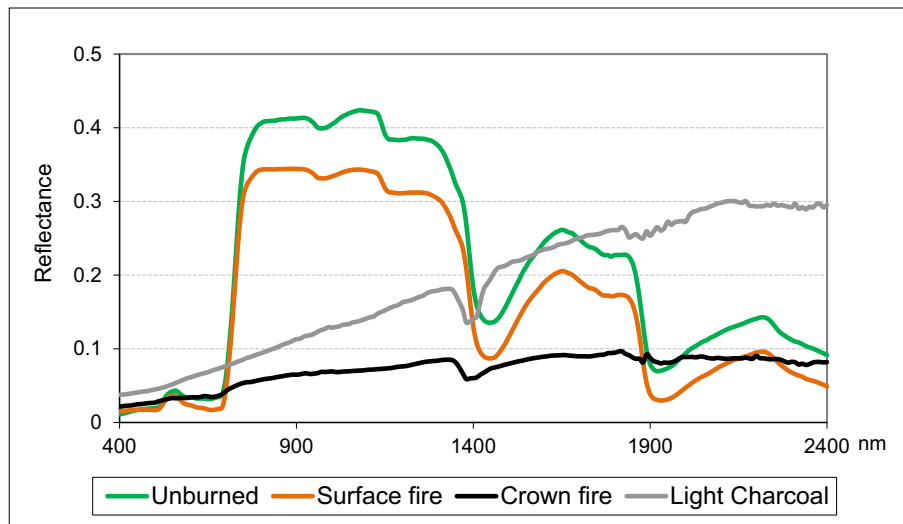


Fig. 1. Reflectance spectra for unburned vegetation canopy and fires affecting different vegetation strata. Spectra were simulated using Prospect + Geosail models.

the fire, and therefore the actual severity of fire impacts. Combustion completeness mainly depends on wind speed, terrain slope, pre-fire biomass load and structure, and water content (Fearnside et al., 2001; van Leeuwen et al., 2014; Ward et al., 1996; Kane et al., 2015). The more intense the fire, the more complete the combustion, and the more important the spectral contribution of ash and charcoal compared to green vegetation. In addition, the type of combustion (smoldering or flaming) impacts the proportion of ash over charcoal in the post-fire signal.

Finally, the temporal difference between fire extinction and image acquisition is critical for detecting BA. This is especially true for tropical regions, which tend to have high cloud cover and rapid vegetation regeneration (Sader et al., 1990). On the contrary, in boreal forests the post-fire signal remains strong for long periods, even several years after burning (Kasischke, 2000). In recent burns, the most important spectral components will be ash and charcoal on the soil layer, and a mixture of green and brown leaves in the surface and canopy vegetation, depending on fire intensity and combustion efficiency. For older burns, post-fire regeneration and the effects of rainfall and wind will reduce the ash and charcoal signal, and only a loss of biomass will make it possible to discriminate BA from unaffected areas (Chuvieco et al., 2006). A brief review on the characteristics of spectral changes caused by fire in different spectral domains follows.

3.1. Solar domain

The solar domain includes the spectral region where reflected solar radiation dominates the signal detected by remote sensing systems: from 0.4 to 2.5 μm . It includes the visible light (blue, green and red: BGR), the near infrared (NIR) and the short-wave infrared (SWIR) bands. Reflectance in these bands is determined by solar energy reflecting from different land surfaces and covers, which is related to their chemical (e.g., pigments, water, dry matter) and physical (e.g., roughness and geometrical arrangement) characteristics, as well as the observation and illumination angles (e.g., bidirectional reflectance distribution function (BRDF) effects). Atmospheric and terrain effects can also affect the detected signal.

Several authors have shown that the NIR and SWIR spectral regions are the especially sensitive to fire effects (López García and Caselles, 1991; Oliva et al., 2011; Pereira et al., 1999; Pleniou and Koutsias, 2013; Trigg and Flasse, 2001). Fire causes both a reduction in leaf area index (when leaves are burned) and/or leaf's pigment reduction and desiccation (when leaves are scorched). The former effects are mostly observed as a strong decrease of the NIR reflectance after burning

(Chuvieco and Congalton, 1988; López García and Caselles, 1991; Silva et al., 2004), while the dryness results in an increase in the SWIR reflectance (Ceccato et al., 2001; Chuvieco et al., 2006; Trigg and Flasse, 2000). Little sensitivity to fire effects has been detected in the visible bands (Fuller and Rouse, 1979; Tanaka et al., 1983), although some studies found them useful to monitor post-fire regeneration, particularly in areas with bright soils (Siljeström and Moreno, 1995).

The decreasing values in NIR reflectance were used in a pioneer study of Hall et al. (1980) to estimate burn severities in a temperate forest. Several authors found that charcoal reflectance in the NIR band was the lowest of all cover types, except when water was present (Chuvieco and Congalton, 1988; Tanaka et al., 1983). The persistence of this post-fire signal contrast is very short in tropical ecosystems (1–3 weeks) (Trigg and Flasse, 2000), while in boreal and temperate regions it may last up to several years after fire (Kasischke and French, 1995).

The increase of SWIR reflectance after fires was first observed in Mediterranean forests (Chuvieco and Congalton, 1988; López García and Caselles, 1991), and was later confirmed in savanna ecosystems, although in these regions the longer SWIR wavelengths (2–2.2 μm) were more sensitive than the shorter SWIR wavelengths (1.4–1.6 μm) (Eva and Lambin, 1998; Trigg and Flasse, 2000). This was also observed in temperate ecosystems (van Wagendonk et al., 2004; Veraverbeke et al., 2011). In actively burning areas, the most sensitive band to radiant emittance is the middle infrared band (MIR: 3–8 μm), although the SWIR radiance also greatly increases when fires are active, which makes it possible to use medium resolution sensors (10–80 m), for active fire detection (Chuvieco and Congalton, 1988), such as Landsat Operational Land Imager (OLI) or Sentinel-2 Multispectral Instrument (MSI) (Schroeder et al., 2016).

The sharp decrease in the NIR reflectance and moderate increase in the SWIR reflectance has been used to generate different spectral indices for detecting burned areas and/or burn severities. Initial efforts were based on the normalized difference vegetation index (NDVI) which was used by Jakubauskas et al. (1990) to estimate three levels of burn severity. Later studies found little sensitivity of NDVI to discriminate burned and unburned areas, particularly in tropical ecosystems (Pereira, 1999). As an alternative to NDVI, several non-linear spectral indices based on the NIR-R space were proposed for BA discrimination, such as the global environmental monitoring index (GEMI: Pinty and Verstraete, 1992), that worked well in tropical ecosystems (Barbosa et al., 1999a; Pereira, 1999), or the burned area index (BAI: Chuvieco et al., 2002; Martín and Chuvieco, 1998).

However, spectral indices combining the NIR-SWIR bands are more

effective for BA discrimination than those based on the NIR-R bands. The normalized ratio of the NIR and SWIR bands was first proposed by López García and Caselles (1991) and later named the “normalized burned ratio” (NBR: Key and Benson, 1999). The NBR and the multi-temporal versions of this index (dNBR, for instance) have been widely used in burn severity estimation (Brewer et al., 2005; Eidenshink et al., 2007; French et al., 2008; Jin et al., 2012; Veraverbeke and Hook, 2013), forest disturbance detection (Wulder et al., 2009); and changes in forest attributes such as biomass (Pflugmacher et al., 2012). Wilson and Sader (2002) proposed the normalized difference moisture index (NDMI) by replacing Landsat Thematic Mapper (TM) band 7 (2.09–2.35 μm) in the NBR with band 5 (1.55–1.75 μm). It produced generally similar results, and the two indices have considerable correlation. Other indices using the NIR and SWIR bands for burned detection are the mid-infrared burn index (MIRBI: Trigg and Flasse, 2001) or the modified burned area index (BAIM: Martín et al., 2006; Quintano et al., 2011). The most recent version of the NASA BA product is also based on a NIR-SWIR detection index (Giglio et al., 2018).

3.2. Middle infrared and thermal domain

The middle infrared and thermal domain includes the spectral region where Earth outgoing radiation dominates the signal detected by remote sensing systems: from 2.5 to 14 μm . It includes the middle infrared (MIR: 2.5–8 μm) and thermal infrared (TIR: 8–14 μm) bands. For this band, the detected signal is related to how different surfaces emit energy, which is mainly related to their temperature and emissivity. As in the solar domain, the signal is also affected by atmospheric transmittance.

The MIR has been extensively used to detect active fires which have much higher emittance than the non-burning background. This was clearly stated in the late 1980s after pioneering studies from the National Oceanographic and Atmospheric Administration (NOAA) (Matson et al., 1984). Later in the 1990s, the contrast in the MIR and TIR radiances between active fires and the background made it possible to create the first global fire products based on Advanced Very High-Resolution Radiometer (AVHRR) images (Ahern et al., 2001; Dwyer et al., 2000a).

In terms of BA, the MIR channel has not been widely used, except for a few attempts to extract the reflective component of the MIR radiance and use it in combination with other optical bands. This was the basis of the GEMI3 index, proposed by Pereira et al. (1999) for detecting BA in AVHRR images. A similar index was used to detect burned pixels in AVHRR Pathfinder images (Carmona-Moreno et al., 2005) and to map forest fires in Greece from AVHRR high-resolution picture transmission images (Vafeidis and Drake, 2005). An optimized version of the MIR/NIR ratio was developed by Libonati et al. (2011) over the Brazilian cerrado.

The thermal contrast between burned and unburned areas was explored by Asrar et al. (1988) and López García and Caselles (1991) to map recent forest fires. They found a significant increase in temperature (5–6° C) for recent burns in temperate forest. This thermal difference vanishes rapidly as vegetation regeneration proceeds. Hope and McDowell (1992) used a combination of surface temperature and vegetation indices to discriminate burned and unburned grasslands. Cahoon et al. (1994) used thermal data for classifying BA from AVHRR images. Goodwin and Collett (2014) used Landsat TM thermal channels along with several spectral indices to discriminate savanna fires in Australia. Finally, Hawbaker et al. (2017) found the Landsat thermal band to be more important than other Landsat bands and spectral indices for detecting BA across the conterminous US.

3.3. Microwave domain

The microwave domain (1 mm–1 m) is generally independent from atmospheric effects. It is commonly sensed by active systems, as the

natural emittance in these wavelengths is quite weak. Synthetic aperture radar (SAR) systems have the capacity to provide data day and night in this spectral region by emitting microwave pulses and recording the radiation scattered back (i.e. backscatter) from the surface (Lewis and Henderson, 1999). Modern SAR systems can measure both, the backscatter coefficient, related to target scattering properties, and the scattering phase, related to the distance between the sensor and the target. Through interferometric SAR (InSAR) processing, the elevation may be computed using the difference in phase between image pairs. As a byproduct, the interferometric coherence (or coherence) is computed. The coherence provides a means to estimate the correlation between the backscattered signal from a given target seen under two slightly different acquisition geometries and offers additional information on scene properties. Lastly, the availability of fully polarized (VV, HH, VH, and HV polarizations) datasets allows for a complete description of the scattering process with polarimetric target decomposition techniques being designed to enhance or suppress contributions from specific scattering mechanisms thus allowing for improved retrieval of the biophysical characteristics of interest. The use of SAR-based techniques provides distinct advantages over other sensor types including sensitivity to vegetation structure and frequent cloud-free acquisitions.

Different wavelengths such as X-, C-, and L-bands (i.e., 2.4–3.75, 3.75–7.5, and 15–30 cm, respectively) have been used in vegetation related studies as radar sensitivity to vegetation characteristics is wavelength and polarization dependent (Dobson et al., 1992; Le Toan et al., 1992; Rignot et al., 1994). Stronger relationships between radar backscatter and vegetation structure were generally found for longer wavelengths and cross-polarized (HV and VH polarizations) channels when compared to shorter wavelengths and co-polarized (HH and VV polarizations) channels (Pulliainen et al., 1994; Sandberg et al., 2011; Tanase et al., 2014; Tanase et al., 2010a). Fires induce variations of the backscatter coefficient that mostly depend on vegetation structure and moisture, but is also influenced by soil moisture (Kasischke et al., 2007). Combustion reduces the number of vegetation scattering elements potentially reducing the backscatter coefficient. However, combustion may also increase scattering from the ground due to reduced signal attenuation and the increased effects of soil surface properties (Kalogirou et al., 2014; Tanase et al., 2010b). Such contrasting effects may generate a wide range of backscatter behavior depending on the interplay between the SAR sensor characteristics, fire impact, and meteorological conditions (Bourgeau-Chavez et al., 2002; Huang and Siegert, 2006; Imperatore et al., 2017; Kasischke et al., 1994; Lohberger et al., 2018; Polychronaki et al., 2013; Ruecker and Siegert, 2000; Tanase et al., 2010b).

4. Historical approaches to BA mapping

The application of satellite images to BA mapping has a long history in remote sensing studies starting in the early 1970s and 1980s and it is still an active research topic employing advanced techniques that integrate geo-statistics, object oriented and machine learning methods. During this period of more than four decades, a wide range of techniques and algorithms have been developed and applied in BA mapping. A brief description of sensors and techniques used in those first decades (1980–2000) follows.

4.1. Sensors for early mapping of BA

The first BA products derived from satellite data relied on medium resolution sensors, mainly Landsat multispectral scanner (MSS) and, after 1982, TM images. Pioneer works were presented at technical conferences or in peer-reviewed journals (Hitchcock and Hoffer, 1974; Hall et al., 1980; Isaacson et al., 1982). These studies emphasized the spectral change associated with fire impacts, particularly in the NIR. The availability of TM images with SWIR and TIR bands increased the potential of using satellite data for BA retrieval. Classification methods

were applied to detecting burned pixels with satisfactory results (Chuvieco and Congalton, 1988; Milne, 1986; Smith and Woodgate, 1985; Tanaka et al., 1983). The earliest attempts to detect levels of damage were also introduced in the early 1980s (Hall et al., 1980), as well as early proposals to use SWIR and TIR radiances for active fire detection (Ambrosia and Brass, 1988; Chuvieco and Congalton, 1988). Spectral indices to emphasize the BA signal over the unburned surroundings from TM images were also suggested in the early 1990s (Jakubauskas et al., 1990; López García and Caselles, 1991). Later that decade, the use of Landsat TM images for estimating fire severity was first proposed (White et al., 1996). A few papers were also published on mapping BA and active fires from visual analysis of spaceborne camera photographs (Furyaev, 1985; Furyaev et al., 1985; Helfert and Lulla, 1990).

Other medium resolution sensors used in BA mapping were the *Haute Résolution Visible* (HRV) sensor, on board the *Système Probatoire d'Observation de la Terre* (SPOT) satellite since 1986, which provided good results in local studies (Eastwood et al., 1998), and the wide field sensor (WIFS) – linear imaging and self-scanning sensor (LISS), onboard the Indian Remote Sensing (IRS) satellite (Vázquez et al., 2001). Radar studies were also published in the 1990s, based mostly on European Remote Sensing (ERS) acquisitions (Bourgeau-Chavez et al., 1997; Kasischke et al., 1992; Landry et al., 1995).

Coarse resolution sensors were mainly used to analyze fire activity over large regions. A pioneering work was published by Brazilian scientists on the impacts of fire in the Amazonian region based on AVHRR images (Setzer and Pereira, 1991). Almost simultaneously, several other papers were published from Canadian, US and Russian researchers on fire effects in the boreal forest also using AVHRR (Cahoon et al., 1992; Gutman et al., 1995; Kasischke et al., 1993). In the same decade, AVHRR was used to map savanna fires in Africa (Barbosa et al., 1999b; Langaas, 1992), Brazil (Pereira and Setzer, 1993) and Mediterranean forest (Chuvieco and Martín, 1994a; Martín and Chuvieco, 1993; Caetano et al., 1996). AVHRR-based studies were also developed to generate active fire information in the mid-1980s (Flannigan and Vonder Haar, 1986; Matson and Holben, 1987; Muirhead and Cracknell, 1985), and later on were the basis of the first global fire product, the world fire web, which mapped active fires and it was operational from 1992 to 1993 (Dwyer et al., 2000b; Stroppiana et al., 2000).

Further developments tried to obtain global BA products from AVHRR images. Since the full resolution data (approximately 1.21 km² at nadir) of this sensor was not centrally archived, these global scale projects used degraded versions of AVHRR images. The most common were the Pathfinder 8 km Land (PAL) used to obtain a global analysis of spatial and temporal patterns of fire occurrence (Carmona-Moreno et al., 2005; Riaño et al., 2007), and more recently the Land Long Term Data Record (LTDR) with 5 km pixel size (Moreno Ruiz et al., 2014; Moreno Ruiz et al., 2012).

Other coarse resolution sensors used in BA mapping were the Along Track Scanning Radiometer (ATSR), VEGETATION and those in geostationary satellites. The ATSR on board the European Remote Sensing (ERS-1 and 2) satellites since 1991 was first used to map African BA (Eva and Lambin, 1998), and afterwards to generate one of the first global BA products, the European Space Agency's (ESA GLOBSCAR in the early 2000s (Simon et al., 2004). The VEGETATION instrument (VGT), onboard the SPOT satellite since 1998, was first used to map BA in Canada (Eastwood et al., 1998; Fraser et al., 2004) and later on served to generate the global burned area 2000 product (GBA2000; Tansey et al., 2004a). Natural Resources Canada implemented two national forest fire management information systems, namely the Canadian Wildland Fire Information System (CWGIS) and the fire monitoring, mapping and modeling system (Fire M3) (Lee et al., 2002). Fire M3 was designed for monitoring daily fire activity for the production of fire maps, fire impact modeling and the dissemination of the generated information. Fire M3 used AVHRR and VGT data to map burned areas,

which were calibrated and verified by medium- to high-resolution imagery such as Landsat TM and SPOT-HRV. A few studies were also developed from images of geostationary satellites such as the Geostationary Operational Environmental Satellite (GOES) (Prins and Menzel, 1992; Prins and Menzel, 1994) and Meteosat (Boschetti et al., 2003), taking advantage of their high temporal frequency (<30 min).

4.2. Early BA mapping methods

For the methods developed and applied in BA mapping, Koutsias et al. (1999) proposed a classification scheme that identified three general groups depending first on whether multi-temporal or single date satellite images were employed, second on whether the output was a direct estimate of BA or an intermediate enhanced product, and third on the type of classification methods. In addition to digital interpretation, the first BA studies also used visual analysis, profiting from the ability of the interpreter to consider very subtle color gradations as well as texture and contextual information. For instance, Chuvieco and Congalton (1988) used visual analysis of Landsat TM images to create reference fire perimeters to validate supervised maximum likelihood classification of a Mediterranean large fire. Visual analysis was also used to delineate fire patches from radar images (Bourgeau-Chavez et al., 1997; Bourgeau-Chavez et al., 2002; Siegert and Ruecker, 2000).

Multi-temporal approaches have the advantage over single post-fire images of reducing commission errors caused by dark soils, water bodies, topographic shades, or cloud shadows. Therefore, the BA detection utilized information not only from spectral but also from temporal changes between the pre- and post-fire satellite imagery. However, multi-temporal approaches can also have several difficulties related to radiometric and geometric adjustments, as well as the discrimination of fire-caused changes from other types of temporal change, such as seasonal floods, harvesting or deforestation.

The second group of the techniques reduces the dimensionality of the original images. This was the case of principal component analysis or vegetation indices, which aimed to improve spectral separability of burned versus other covers. Single channel density slicing, and thresholding of spectral vegetation indices were also very common techniques for BA discrimination, both with SAR imagery (Kasischke et al., 1994) and AVHRR data (Martín and Chuvieco, 1993). For the single channel density slicing method, researchers were slicing the histogram for getting different levels of severity within the fire perimeter. Several spectral indices were used, including the NDVI, the Soil Adjusted Vegetation Index (SAVI), the GEMI and the BAI (Chuvieco and Congalton, 1988; Chuvieco et al., 2002; Chuvieco and Martín, 1994a, 1994b; Koutsias and Karteris, 2000; Viedma et al., 1997). In these cases, usually the spectral signal of pre- and post-fire image was compared because of sharp changes in the spectral signal observed in specific spectral channels following the fire. Principal component analysis (PCA) has been used since early 1980s for BA and change detection analysis (Richards, 1984). Several approaches used PCA in BA mapping from: (i) an 8-dimensional multi-temporal image dataset consisting of two Landsat MSS scenes (Richards, 1984), (ii) a standardized PCA on a 12-dimensional multi-temporal image dataset consisting of two Landsat TM scenes, and a subset of spectral channels consisting of pairs of two spectral channels with low to medium correlation (Pereira 1992), (iii) multi-temporal ERS-2 SAR images acquired before and after the fire event (Siegert and Ruecker, 2000), (iv) a non-standardized PCA on a multi-temporal dataset comprising TM bands 3, 4, and 5 from both dates (García-Haro et al., 2001), (v) a dataset consisting of a standardized NDVI, surface temperature and albedo from a NOAA AVHRR time series dataset (Nielsen et al., 2002), (vi) a standardized PCA along with a simple, non-parametric, supervised classification (parallelepiped) on a Landsat time series dataset consisting of 22 annual images of Landsat MSS, TM and Enhanced Thematic Mapper Plus (ETM+) from 1972 to 2002 (Hudak and Brockett 2004), and (vii) a forward/backward principal component analysis of Landsat-7 ETM+ data to enhance the

spectral signal of burned areas (Koutsias et al., 2009).

Finally, the third group of studies refers to the classification techniques, on whether supervised and unsupervised methods were used. This depends on the previous knowledge of fire effects in the target region. The maximum likelihood classification and k-means clustering algorithms were employed in several studies either to directly map BA or used to evaluate other classification techniques (Henry 2008; Pereira and Setzer, 1993). Methods based on logistic regression were introduced to map BA using multi-date (Koutsias and Karteris, 1998) and single-date (Koutsias and Karteris, 2000) Landsat TM imagery. The main consideration when implementing BA classifications was to express the classification problem in a binary way, i.e., burned vs unburned pixels. Other approaches, such as spectral mixture analysis (SMA), were first applied in BA mapping in the early 1990s (Caetano et al., 1996).

5. Current EO approaches to detect BA information

Building on the historical developments, BA detection algorithms have been improved in the last ten years, incorporating new processing approaches, as well as new sensors and new integration methods. The review of these recent developments is structured in different spectral domains: passive optical, active radar and LiDAR, with a brief section to comment on integrated methodologies. Table 1 includes a list of sensors from which most available BA products have been obtained.

5.1. Optical sensors

Global BA products rely on sensors that provide very high temporal resolution (daily images, sometimes multiple images each day), and coarse spatial resolution (≥ 250 m pixel size). To cope with the great diversity of worldwide fire conditions and with the potential problems in data acquisition, algorithms need to be robust and spatially adaptable. The first global BA products were based on regional algorithms (Tansey et al., 2004a), which were adapted to different fire conditions (boreal, tropical forest, grasslands, etc.). The main problems in this approach were the impacts of borders between regions and the potential variations of accuracy among ecosystems (Humber et al., 2018). For this reason, local-adapted or physically based approaches have been more common in the last years for global BA algorithms. The former aim to discriminate burned from unburned pixels based on a set of attributes (reflectance bands or spectral indices) from which discriminant functions are created by maximizing inter-class and minimizing intra-class variation. Examples are Bayesian classifiers (Riaño et al., 2007), random forests (Ramo and Chuvieco, 2017), and support

vector machines (SVM) (Cao et al., 2009) approaches.

The most common methods for global BA mapping have been based on physically based rules that discriminate burned pixels from unburned. Additional spatial and temporal conditions are included to cope with the global diversity of fire conditions. This approach was the basis of one of the first global BA products derived from AVHRR pathfinder data (Carmona-Moreno et al., 2005). A similar approach has been later refined to generate the MODIS MCD64A1 (Giglio et al., 2018) and FireCCI50 (Chuvieco et al., 2018) products. In both of these 2018 studies, the algorithms integrate reflectance changes with active fire observations (hotspots, HS) obtained from thermal anomalies. Another way of including a physical model in BA detection is the use of BRDF correction models. These models aim to reduce the impact of illumination and observation geometry in the estimated reflectance. BRDF models have been used to estimate the post-fire reflectance ($t + 1$) from the pre-fire conditions (t) and compare it with the actual $t + 1$ reflectance. When the difference between the modeled and the measured reflectance exceeds a certain threshold, it is assumed that it indicates significant changes in cover conditions. This approach is used for NASA's MCD45A1 BA product (Roy et al., 2005; Roy et al., 2008).

Regional or national products have been developed in the recent years based on medium resolution sensors, taking advantage of the improvements in processing power and the free access to Landsat and Sentinel-2 acquisitions. Previous use of Landsat images for BA mapping was local, and the methods were difficult to generalize to other regions. The public release of the Landsat archive by the USGS in 2008 (Loveland and Dwyer, 2012) initiated a new era for using medium resolution sensors for regional (or even global) retrieval of BA, as it provided a wealth of freely available images, both covering large territories and for a long period of time.

In terms of methodological developments, the availability of Landsat time series made it possible to develop dedicated time-series detection methods for these images. They were initially applied to detect forest changes, but they have also been used for monitoring BA. These methods include the Vegetation Change Tracker (VCT) (Huang et al., 2010) and the Landsat-based detection of Trends in Disturbance and Recovery (LandTrendr) (Cohen et al., 2010; Kennedy et al., 2010), which divide annual time series of spectral responses into piecewise segments, and then use the changes between segments and characteristics of segments to delineate disturbances. In a further elaboration, Cohen et al. (2018) used the Random Forests algorithm to combine an ensemble of the LandTrendr results for different bands and indices into a single analysis. Similarly, Schultz et al. (2016) proposed and tested a methodology to fuse disturbance maps derived from different indices using the Breaks for Additive Seasonal and Trend (BFAST) algorithm,

Table 1
Satellite sensors used for burned area mapping. See the Annex A for acronym descriptions.

| Satellite (sensor) | Operator | Operational dates | | Temporal resolution | Spatial resolution |
|-----------------------------|-----------|---|-------------------|---------------------|----------------------------|
| | | Launch date | End operation | | |
| ENVISAT (MERIS) | ESA | March 1, 2002 | May 9, 2012 | 2–3 days | 300–1200 m |
| JPSS (VIIRS) | NOAA | October 28, 2011 | Still operating | 1–2 days | 375–750 m |
| Landsat 1–3 (MSS) | NASA/USGS | July 23, 1972 | September 7, 1983 | 18 days | 80 m |
| Landsat 4–5 (TM) | NASA/USGS | July 16, 1982 | June 5, 2013 | 16 days | 30–120 m |
| Landsat 7 (ETM+) | NASA/USGS | October 5, 1993 | Still operating | 16 days | 15/30–60 m |
| Landsat 8 (OLI/TIRS) | NASA/USGS | February 11, 2013 | Still operating | 17 days | OLI: 15/30 m TIRS: 100 m |
| NOAA-7-19 (AVHRR) | NOAA | Oct 19, 1978 | Still operating | 1–2 days | 1100 m |
| PROBA V | ESA | May 7, 2013 | Still operating | 1–2 days | 300 m |
| Sentinel 1A-B (SAR) | ESA | April 3, 2014 (1A) April 25, 2016 (1B) | Still operating | 6 days | 5–20 m |
| Sentinel 2A-B (MSI) | ESA | June 23, 2015 (2A) March 7, 2017 (2B) | Still operating | 5 days | 10–20–60 m |
| Sentinel 3A-B (SLSTR, OLCI) | ESA | 16 February 2016 (3A) 25 April 2018 (3B) | Still operating | 1–2 days | 300 m OLCI, 500 m SLSTR |
| SPOT 1–7 (HRV) | CNES | February 22, 1986 | Still operating | 26 days | 2.5 to 20 m |
| SPOT 4–5 (VGT) | CNES | March 24, 1998 | July 2013 | 1–2 days | 1000 m |
| Terra-Aqua (MODIS) | NASA | December 18, 1999 (Terra) May 4, 2002 (Aqua) | Still operating | 1–2 days | 250–1000 m |

which iteratively decomposes the observed time series into a trend, seasonal pattern, and residual component, with detection of sudden changes (DeVries et al., 2015; Verbesselt et al., 2010). Other approaches decomposed dense time series to separate seasonality and long-term trends and detect change as departure from those trends using Landsat data (Brooks et al., 2014; Zhu and Woodcock, 2014). Finally, others have detected change using decision trees with predictors characterizing the entire Landsat time series (Hansen et al., 2014). All of these methods detect abstract land change and require additional attribution to characterize the specific type of change, such as BA (Schroeder et al., 2017; Zhao et al., 2015).

Change-detection algorithms specific to mapping BA across the full Landsat archive have also emerged. Using all available Landsat data for Queensland, Australia, Goodwin and Collett (2014) combined decision rules with a region-growing algorithm to identify areas of change and then classified which of those areas of change were caused by fire. In forested parts of the western US, Boschetti et al. (2015) identified areas of spectral change using composites of Landsat 7 ETM+ data from 2002 and then used MODIS active fire data to separate BA from other types of change. These two studies were the first to demonstrate that large territories can be routinely mapped from Landsat data with semi-automated approaches and paved the way for the development of the U.S. Geological Survey's Landsat Burned Area Essential Climate Variable (BAECV) (Hawbaker et al., 2017). The BAECV algorithm was developed to consistently map burned areas ≥ 4 ha across the conterminous U.S. regardless of ecosystem type using all available Landsat data by combining a gradient boosted classifier with thresholding and region growing.

Landsat-based studies also set forth the development of approaches to map BA using data from the Sentinel-2A and 2B missions, which provide free accessible images, in 13 spectral channels (from 10 to 60 m of spatial resolution) and with a combined 5-day coverage period. Using Sentinel-2 images, Roteta et al. (2019) have been recently able to map BA for the whole Sub-Saharan Africa including all Sentinel-2A acquisitions for 2016. The accuracy of this BA product significantly improved that obtained from coarse resolution sensors, particularly in detection of small burns (<100 ha). Landsat and Sentinel-2 images have also been used in conjunction to estimate burn severity (Mallinis et al., 2018).

In addition to time series analysis, recent techniques for BA mapping using medium resolution sensors have relied on new classification approaches, such as fuzzy memberships, object oriented and radiative transfer models (RTM). Fuzzy approaches have been explored by Stroppiana et al. (2012a) to integrate partial evidence of BA provided by different spectral indices. Variations of spectral mixture analysis (SMA) approaches have been recently proposed, including spectral angle mapper classifiers (Oliva et al., 2011; Quintano et al., 2013) or the Multiple Endmember Spectral Mixture Analysis (MESMA), which allows more than two endmembers (Roberts et al., 1998). The key success factor in SMA and MESMA is to provide a suitable library of spectra for well-chosen endmembers. They can be specified in advance or be derived from known pixels within the image. Fernandez-Manso et al. (2016) used MESMA to delineate BA and estimate fractions of the endmembers, although it was not clear if the results were superior over other approaches (e.g., index-based). Since burn conditions are quite diverse, data mining techniques have been recently proposed to select the most adequate inputs for generating machine learning classifiers (Ramo et al., 2018).

Object-based image analysis (OBIA) constitutes an alternative classification technique to the pixel-by-pixel approach and has become quite popular in the field of remote sensing (Benz et al., 2004). OBIA has been used successfully to map BA (Gitas et al., 2004; Mitri and Gitas, 2010; Polychronaki and Gitas, 2010), reducing common errors found in pixel-based multispectral classifications (Weih and Riggan, 2010), and mitigating spectral overlapping between burned and other land cover classes (Mitri and Gitas, 2004). In addition, the 'per-object'

approach facilitates the synergy between advanced image analysis techniques (e.g. feature selection methods) and classification methods, resulting in thematic maps of higher accuracy (Dragozi et al., 2014). Even though most OBIA studies were primarily focused on high-spatial resolution images (Dragozi et al., 2014; Polychronaki and Gitas, 2012), these methods have been successfully used with coarser resolution data such as AVHRR (Gitas et al., 2004) or MODIS (Mohler and Goodin, 2012).

Another recent approach to BA discrimination has been the use of physical-based models (radiative transfer models: RTM), which have been mostly addressed towards burn severity estimation. Forward simulation implies generating a set of realistic conditions from RTM, while inverse modeling implies comparing satellite measured reflectance with modeled reflectances. The input variables used to obtain the most similar modeled to actual pixel reflectance are then assigned to each pixel. Both forward and backward simulations have been performed, trying to obtain realistic scenarios of post-fire conditions. These model scenarios were based on simulating Composite Burned Index (CBI) values. CBI is a widely used protocol to estimate field severity (Key and Benson, 2006). The simulation was obtained with a two-layer RTM, which accounted for average values of leaf area index and leaf pigment changes caused by the fire (Chuvieco et al., 2006). The model was later applied to estimating CBI values for several large fires in Spain (De Santis and Chuvieco, 2007; De Santis et al., 2009) and coastal California (De Santis et al., 2010). Since the retrieval of CBI values from satellite data may be greatly affected by fraction of forest cover, De Santis et al. (2009) proposed a modification of the original CBI method to take into account this variable.

Finally, to balance commission and omission errors, several classification approaches propose to detect BA in two phases: the first one would be addressed to reduce commission errors by classifying only the most clearly burned pixels, while the second would aim to reduce omission errors, by adding to the first-stage detected pixels those neighbors that have similar spectral characteristics (Alonso-Canas and Chuvieco, 2015; Bastarrika et al., 2011a; Bastarrika et al., 2011b; Chuvieco et al., 2008; Stroppiana et al., 2012b).

5.2. Radar

Burned area detection from SAR data was frequently employed over tropical areas characterized by persistent cloud cover (Lohberger et al., 2018; Siegert and Ruecker, 2000; Verhegghen et al., 2016) or at high latitudes where low sun angles hindered observations with optical sensors (Bourgeau-Chavez et al., 1997; Bourgeau-Chavez et al., 2002; Goodenough et al., 2011; Kasischke et al., 1994; Kasischke et al., 1992). Other studies used change-detection frameworks coupled with non-parametric classifiers (Gimeno and San-Miguel-Ayanz, 2004), object-based classification methods (Lohberger et al., 2018; Polychronaki et al., 2013), empirically derived thresholds (Verhegghen et al., 2016) or region-growing algorithms (Imperatore et al., 2017) to detect the BA. Few studies used the C-band interferometric coherence to delineate fire scars in tropical environments. Such studies used empirically derived thresholds applied to temporal differences of pre- and post-fire coherence estimates (Liew et al., 1999). More recent studies focused on radar polarimetric properties (Goodenough et al., 2011) and integrating radar and optical datasets within common detection algorithms (Stroppiana et al., 2015) or through integration of the radar and optically detected burned areas (Verhegghen et al., 2016). Such studies demonstrated that fires result in ambiguous effects depending on the radar wavelength, polarization, and meteorological conditions at image acquisition (Lohberger et al., 2018; Ruecker and Siegert, 2000) (Imperatore et al., 2017; Polychronaki et al., 2013; Tanase et al., 2010b) (Bourgeau-Chavez et al., 2002; Huang and Siegert, 2006; Kasischke et al., 1994) (Gimeno and San-Miguel-Ayanz, 2004) (Menges et al., 2004).

SAR data were also used to estimate fire impacts from the

backscatter coefficient (Kurum, 2015), the interferometric coherence (Tanase et al., 2010a) or through polarimetric decomposition techniques (Tanase et al., 2014). Most studies used post-fire images (Bourgeau-Chavez et al., 1994; Tanase et al., 2010a; Tanase et al., 2010b) or change detection frameworks based on pre- and post-fire datasets (Kurum, 2015; Tanase et al., 2015b) while few authors focused on the synergy between optical and radar sensors (Tanase et al., 2015a). The most accurate results were obtained using the cross-polarized (HV) backscatter and longer wavelengths such as the L-band with the retrieval accuracy being negatively influenced in areas of steep topography or with high soil moisture (Kalogirou et al., 2014; Kasischke et al., 2007; Tanase et al., 2010b). The influence of topography was removed through change detection approaches while the use of datasets acquired under dry environmental conditions or multi-temporal averages were suggested to reduce the effect of varying soil and vegetation moisture content (Tanase et al., 2015b; Tanase et al., 2010a). In addition, the dependency of in situ data for modeling was eliminated by using polarimetric decomposition techniques (Tanase et al., 2014). However, the scarcity of full polarimetric acquisitions has precluded the use of polarimetric analysis over large areas.

5.3. Lidar

An appropriate evaluation of the impact of the fire on the vegetation would require pre- and post-fire LiDAR acquisition. Since most of the available data are airborne, there is a scarcity of studies based on the bitemporal acquisitions (McCarley et al., 2017a,b). Therefore, the use of LiDAR data for fire effects assessment commonly relies on comparing the affected areas to adjacent unburned areas or combined with bitemporal multispectral data (Montealegre et al., 2014).

Most of published studies rely on the CBI to estimate post-fire effects from airborne LIDAR data. Wang and Glenn (2009) estimated CBI values over a sagebrush rangeland in the U.S. from bitemporal LiDAR data as the difference in mean vegetation height over 5×5 m cells. Height differences were classified into three burn severity levels (low to high) using ≥ 100 field samples to establish the height difference threshold for each level. Montealegre et al. (2014) calibrated a logistic regression model to relate post-fire LiDAR metrics to field CBI measures over Mediterranean forests in Spain. The output probabilities of the model were further grouped into different burn severity levels.

Several studies have used a combined approach of airborne LIDAR and passive sensors to estimate post-fire effects. Kwak et al. (2010), for instance, used LiDAR data to estimate the degree of physical damage (loss of canopy cover), while NDVI values from a multispectral sensor were used to determine the biological damage (vegetation vitality). Physical and biological damage were subsequently combined to classify the affected area into four levels of fire damage. Structural changes in the forest cover related to fire effects were retrieved by McCarley (2017a) from a bitemporal LiDAR dataset along with several spectral indices derived from Landsat data in a temperate coniferous forest in the U.S. The best relationships between multispectral and LiDAR data occurred for changes in canopy cover whereas the relationships with LiDAR metrics representing changes in mid and lower strata weakened and became poorly correlated with those LiDAR metrics representing changes near the surface layer. Wulder et al. (2009) integrated two transects (pre- and post-fire) of data collected with an airborne profiling LiDAR system with Landsat imagery to relate changes in forest structure to post-fire conditions estimated by spectral indices over a burned boreal forest in Canada. Due to the lack of spatial coincidence between the two LiDAR transects, the post-fire image was segmented using an object-based approach and structural metrics were summarized for each segment, representing homogeneous vegetation patches, as well as for the total length of the transects.

Only one study based on satellite LIDAR measurements for BA mapping has been published so far. Goetz et al. (2010) evaluated fire disturbance over boreal forests in Alaska, using ICESat Geoscience Laser

Altimeter System (GLAS) data. Because of observation limitations of this sensor, structural changes were assessed after stratification of the area based on time since fire, vegetation type (deciduous vs. coniferous) and burn severity. Although differences in vegetation height between burned and unburned areas were found to be significant, these authors showed that this metric alone may not be the most adequate to evaluate fire effects since it is affected by regrowth rates in different vegetation types as well as the different burn severity levels.

Very few studies have analyzed the impacts of fire on soil carbon storage. Ballhorn et al. (2009) compared the height difference between burned and adjacent unburned areas along 79 airborne LiDAR transects over peat swamp forests in Central Kalimantan, Borneo, during the 2006 El Niño episode. Soil consumption estimates were in close agreement with field measurements. Reddy et al. (2015) estimated soil consumption by a peat fire in North Carolina and Virginia, USA, based on the elevation change from bitemporal airborne LiDAR datasets and compared the results to consumption values estimated using the First-Order Fire Effects Model (FOFEM). They found LiDAR estimates more accurate than modeled estimates due to the limited representation of peat depth in the LANDFIRE fuel model input layer. Additionally, they analyzed the influence of LiDAR elevation errors in the carbon loss estimates using a Monte Carlo simulation to find out that LiDAR elevation errors did not significantly contribute to the uncertainty in the soil carbon loss. The difference in elevation using pre- and post-fire airborne LiDAR data after elevation matching over invariant targets was used by Alonzo et al. (2017) to compute the consumption of surface litter and organic soils in a boreal forest fire in Alaska, USA. This study showed that elevation over the burned area had statistically significant differences and those differences were more important in areas where deeper organic soils developed.

5.4. Synergetic approaches

In addition to using new sensors and approaches, recent BA products have also taken advantage of integrating different EO techniques to strengthen the discrimination of burned pixels and reduce both omission and commission errors.

The most synergistic approach has been the combined use of thermal anomalies (HS, from MIR and TIR bands) and changes in reflectance from NIR, SWIR and visible bands. The former identifies active fires while the latter detects BA. Thermal amplification caused by active fires is very distinct and helps to identify burning pixels, while the post-fire signal of charcoal and scorched vegetation last longer and cover the whole area affected by fire. The former avoids potential commission errors (discriminating those reflectance changes most likely to be actual fires), while the latter helps delineating the whole area affected by the fire (not just the burning pixels) and therefore aids to reduce omission errors. Typically, before running a hybrid BA algorithm, the HS are filtered to remove stable thermal anomalies, which are commonly associated with power stations, volcanos or gas flares. Then, HS are used to discriminate between actual BA and the surroundings, reducing the potential confusions caused by reflectance changes that are unrelated to fire (such as seasonal floods, cropping, deforestation, etc.). Hybrid algorithms were first proposed 20 years ago (Fraser et al., 2000; Roy et al., 1999) and have been since then extensively applied to BA mapping. Two of the most recent global BA products, MCD64A1 from NASA (Giglio et al., 2018), and FireCCI50 from ESA (Chuvieco et al., 2018) used this approach. Hybrid algorithms have also been used with medium resolution data, for instance, merging 1 km MODIS active fire detections and multi-temporal Landsat TM-ETM + images over the western United States (Boschetti et al., 2015). Also, a hybrid algorithm was utilized to map 2016 BA in the whole Sub-Saharan Africa from Sentinel-2 images (Roteta et al., 2019).

Another approach to combine different sensors is the joint use of optical and radar data. Some examples are the study by Stroppiana et al. (2015) centered in Portugal that mapped BA from Landsat and

Envisat-ASAR data, and the analysis of Verhegghen et al. (2016) who used Sentinel-1 and Sentinel-2 images to map BA in Congo by thresholding the differences in pre- and post-fire VV polarization (Sentinel-1) and NDVI and NDWI (Sentinel-2) spectral indices. They found that Sentinel-2 data with their 5-day revisit could effectively map BA in places with frequent cloud cover. However, incorporating radar data from Sentinel-1 improved their results where Sentinel-2 images were obscured by cloud cover.

Integrated analysis of LIDAR and passive optical sensors have also been performed for BA mapping. Garcia et al. (2017), for instance, integrated post-fire LiDAR data and bitemporal Landsat data. Pre-fire biomass was estimated using a two-step approach. First, a LiDAR model was calibrated using field data to estimate biomass over the study area. Second, in order to derive pre-fire biomass values, LiDAR-based estimates across the 2 km buffer were extrapolated over the whole area using pre-fire Landsat data. By comparing pre-fire to post-fire biomass values, it was possible to compute the biomass consumed by the fire.

6. Existing EO-derived BA products

6.1. Global products

After the first attempts to generate global BA products in the late 1990s, the early 2000s provided the mature conditions to release the first global semi-operational BA datasets. Building on the experience of NOAA-AVHRR BA algorithms (Barbosa et al., 1999a; Fernández et al., 1997; Kasischke and French, 1995; Langaas, 1992; Martín and Chuvieco, 1995; Pereira, 1999), the new BA products were mainly based on the MODIS sensors, on board NASA's Terra and Aqua satellites, and the SPOT Vegetation (VGT) sensor (Table 2).

The first global BA product at coarse resolution was produced by the Joint Research Centre of the European Union. It was named Global Burned Area (GBA2000) and was based on daily VGT images acquired throughout the 2000. This product had 1 km² spatial resolution and provided monthly estimates of BA. The BA detections were based on seven regional algorithms adapted to different fire conditions (Tansey et al., 2004b). In parallel to the GBA project, the European Space Agency developed the GLOBSCAR BA product for the same year 2000. This global monthly product was derived from daytime ERS-2 ATSR-2 data with a nominal pixel size of 1 km². BA detection relied on the combination of a contextual and a fixed threshold algorithm (Simon et al., 2004).

Following the experience of GBA, other global BA products have been released by European institutions: the L3JRC (Tansey et al., 2008) covering the period from 2000 to 2007; the Globcarbon (Plummer et al., 2006), from 1998 to 2007, and the Copernicus GIO_GL1_BA products, all at 1 km spatial resolution. All these products were derived from VGT images (in Globcarbon, ATSR images were used as well). The exception is the most recent version of the Copernicus GIO_GL1_BA, which after 2013 has 333 m resolution and is derived from PROBA-V data (https://land.copernicus.eu/global/products/ba, last accessed July 2018).

In a different context, the Fire_CCI project (part of the European Space Agency's Climate Change Initiative) has generated three global BA products over the last few years. The first one was named FireCCI41 and it was based on 300-m resolution MERIS images from the ENVISAT satellite, covering the period from 2005 to 2011. The BA algorithm was a hybrid and two-phase approach, where MERIS reflectances were supplemented with first MODIS HS to detect the most clearly burned pixels and then contextual criteria were applied for improved delineation of burned patches (Alonso-Canas and Chuvieco, 2015; Chuvieco et al., 2016). The most recent products of the Fire_cci project (FireCCI50 and 51) were derived from MODIS 250 m bands (R and NIR reflectance) also supplemented with HS. They cover the full time series of Terra-MODIS (2000–2017) (Chuvieco et al., 2018). The product is publicly available at www.esa-fire-cci.org (last accessed February

Table 2
Overview of global burned area datasets. See the Annex A for a list of acronyms.

| Name of burned area dataset | Time span | Sensor/method | Spatial resolution g = grid p = pixel d = degree | Temporal compositing | Development purpose | Reference |
|-----------------------------|-----------------|--|---|---|--|--------------------------------------|
| GBA2000 | 2000 | SPOT VGT | p:1 km, g:0.25 d, 0.5 d, 1 d | Monthly | Prototype | Tansey et al. (2004a, 2004b) |
| GLOBSCAR | 2000 | ERS2-ATSR2 | p:1 km | Monthly | Prototype | Simon et al. (2004) |
| L3JRC | 2000–2007 | SPOT VGT | p:1 km | Monthly | General purpose | Tansey et al. (2008) |
| GLOBCARBON | 1998–2007 | SPOT VGT, ATSR-2, AATSR | p:1 km; g:10 km, 0.25 d, 0.5 d | Monthly, | Global carbon cycling and climate models | Plummer et al. (2006) |
| GIO-GL1* | 1999-present | SPOT VGT, from 04/2014 onwards: PROBA-V | p:1 km | 10-day composite | GHG reporting | Tansey et al. (2008) |
| GIO-GL1 300* | 04/2014-present | PROBA-V | p:300 m | 10-day composite | GHG reporting | Tansey et al. (2008) |
| FireCCI41 | 2005–2011 | Hybrid: MERIS reflectances guided by MODIS hotspots | p:300 m g:0.25 d | Monthly | Climate and dynamic vegetation models | Chuvieco et al. (2016) |
| FireCCI50 and FireCCI51 | 2001–2017 | Hybrid: MODIS reflectances guided by MODIS hotspots | p:250 m g:0.25 d | Biweekly Monthly | Climate and dynamic vegetation models | Chuvieco et al. (2018) for FireCCI50 |
| GFED4s | 1997-present | Aug-2000 to present: MCD64A1 supplemented by small fire burned area (from scaled hotspots) | g:0.25 d | Monthly with scalars for daily and 3-hourly estimations | Atmospheric and biogeochemical models; | van der Werf et al. (2017) |
| GFED4 | 1995-present | Aug-2000 to present: MCD64A1 before: scaled ATSR or VIRS hotspots | g:0.25 d | Monthly | Atmospheric and biogeochemical models; | Giglio et al. (2013) |
| MCD45A1 c51 | 2000–01/2017 | MODIS bi-directional reflectance (BRDF) temporal trends | p:500 m | Monthly | General purpose | Roy et al. (2008) |
| MCD64A1 c6 | 2000-present | Direct broadcast algorithm Hybrid: MODIS reflectances guided by MODIS hotspots | p:500 m g:0.25 d | Monthly | General purpose | Giglio et al. (2018) |

2019).

NASA has also been very active in generating global BA products. The first one released was the MCD45A1 product derived from 500 m MODIS imagery. This product employed a BRDF model to detect significant differences between observed and predicted daily reflectance data (Roy et al., 2008). This product was the standard NASA BA product from 2000 through 2016, but it has been recently superseded by MCD64A1. In contrast to the MCD45A1 product, the MODIS MCD64A1 product employs a hybrid algorithm that uses both the reflectance changes and the thermal anomalies associated with biomass burning (Giglio et al., 2009). The current version of this algorithm (collection 6) provides considerably more sensitivity than the original and identifies 26% more global BA than previous collection (Giglio et al., 2018). This product is processed from 2000 to the present (https://lpdaac.usgs.gov/dataset_discovery/modis/modis_products_table/mcd64a1_v006, last accessed February 2019).

The MCD64A1 product in combination with additional variables on fuel properties and emission coefficients has in turn been used to produce the Global Fire Emissions Database (GFED). Current versions of the GFED (designated GFED4 and GFED4s) include data from the MCD64A1 collection 5 product, as well as the ATSR sensor for the pre-MODIS era (1995–2000). GFED4s adds an estimation of the area burned by small fires (< 100 ha), which are commonly not detected by global products based on coarse resolution sensors. GFED4s estimates the contribution of those small fires by BA to MODIS active fire hotspots located outside of burned patches mapped in the MCD64A1 BA product. The BA allocated to each “outside-of-burn” hotspot is in turn estimated using postulated relationships between dNBR, the number of “within-burn” hotspots, and the BA actually mapped in the MCD64A1 product (Randerson et al., 2012; van der Werf et al., 2017).

Fig. 2 shows average BA for different global products in the common available years. Even though a full comparison of global BA products is still to be done, those recently performed showed common spatial patterns, particularly in those based on hybrid algorithms that use

common hotspots (Humber et al., 2018; Chuvieco et al., 2018).

6.2. Regional products

Several countries have been operationally developing BA mapping products in the framework of various fire monitoring systems. In the United States, the Monitoring Trends in Burn Severity (MTBS) project was sponsored by the Wildland Fire Leadership Council (WFLC) and implemented jointly with the U.S. Geological Survey (USGS) and Forest Service (Eidenshink et al., 2007). The project's objective was the systematic production of BA maps and associated burn severity information. Among the different data employed by the MTBS project, pre-fire and post-fire Landsat TM, Enhanced TM Plus (ETM+), and OLI imagery are mainly used for the computation of the dNBR and the subsequent generation of estimated burn severities.

The U.S. Geological Survey has also recently developed the Landsat Burned Area Essential Climate Variable (BAECV) project, which covers the conterminous U.S. (Hawbaker et al., 2017). The BAECV algorithm was used to identify burned areas ≥ 4 ha in every Landsat TM and ETM+ images with <80% cloud cover from 1984 through 2015 across the conterminous territory of USA. A modified version of the BAECV algorithm has been developed for use with Landsat OLI data. New Landsat BA products using the modified BAECV algorithm are available through the USGS EarthExplorer (earthexplorer.usgs.gov) interface for Landsat TM, ETM+ and OLI data from 1984-present.

The lack of harmonized BA information and a holistic approach for forest fire prevention in Europe motivated the European Commission services and the relevant fire services of each country to develop the European Forest Fire Information System (EFFIS) (San-Miguel-Ayanz et al., 2012). EFFIS is a comprehensive forest fire management system with its core applications based on remote sensing and geographic information systems (GIS), which currently supports the monitoring of fires in 41 countries in Europe, Middle East and North Africa (<http://effis.jrc.ec.europa.eu>, last accessed September 2018). EFFIS

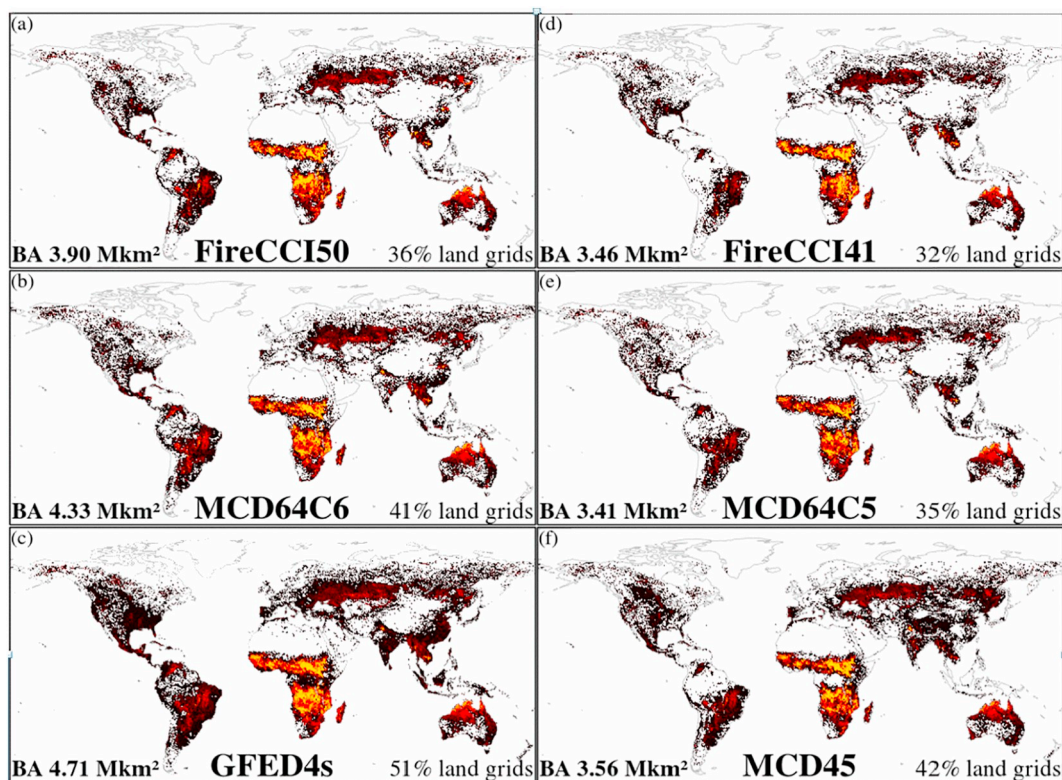


Fig. 2. Annual burned fraction per 0.25-degree grid cell, averaged across 2005 to 2011, for different global burned area products. See the Annex A for a list of acronyms.

incorporates different modules, namely FIRE Danger Forecast, Active Fire Detection, Rapid Damage Assessment and post-fire modules. MODIS data are employed for the detection of hot spots and BA mapping (for fires over 40 ha) on a European scale. Subsequently, this information is integrated into a national GIS for further analysis at a country level. BA products of high resolution are also provided, upon demand, by the Copernicus Emergency Management Service (EMS). This service is based on the rapid acquisition, processing and analysis of satellite imagery and other geospatial datasets after a fire event.

In Mexico and Central America, a semi-operational program to provide information on BA and active fire was established in early 2000s. The system is operated by the National Commission for the Knowledge and Use of the Biodiversity (CONABIO; [Ressl et al., 2009](#)). Hot spots are mapped with AVHRR and MODIS data, following methods of [Flasse and Ceccato \(1996\)](#) and [Giglio et al. \(2003\)](#). BA mapping is derived from NDVI and NBR values computed from MODIS-Aqua data.

The Forest Research Centre in the School of Agriculture at the Technical University of Lisbon in Portugal has developed a national operational BA mapping system based on remotely sensed data. In particular, the system employs time series of Landsat MSS, TM and ETM + data for BA delineation for the time period from 1975 to present. The resulting maps are utilized for structural fire risk mapping and the products are operationally used by the National Forest Authority, the National Authority for Civil Protection and by large private landowners ([Nunes et al., 2005](#); [Oliveira et al., 2012](#)).

In Greece, an Operational Burned Area Mapping (OBAM) service has been developed in the framework of the National Observatory of Forest Fires (NOFFi) project implemented by the Laboratory of Forest Management and Remote Sensing of the Aristotle University of Thessaloniki (AUTH) in collaboration with the Hellenic Ministry of Environment and Energy and financially supported by Greece's Green Fund ([Tompoulidou et al., 2016](#)). The NOFFi-OBAM service is based on an OBIA approach and supervised classification models. Any remote sensing imagery (Landsat 8 OLI, Sentinel-2) can be used in the semi-automated classification which is performed with public domain software.

In Australia, there are automated and semi-automated methods for BA mapping over the rangelands of northern Australia. The Queensland government produces an annual BA map based on the [Goodwin and Collett \(2014\)](#) algorithm. The North Australia and Rangelands Fire Information (NAFI) system is a MODIS-based fire patch mapping system hosted by Charles Darwin University. The NAFI methodology involves differencing pre- and post-fire MODIS imagery with a subsequent segmentation and classification step and some user input (www.firenorth.org.au). For the other parts of Australia, BA mapping has been done ad hoc for some events, using supervised high-resolution satellite imagery, airborne burn mapping, ground-based surveys, or a combination of these methods. However, an automated algorithm for nationwide BA and severity mapping using Geoscience Australia's (GA's) Landsat and Sentinel-2 data cube infrastructure was recently developed and is close to operational. The algorithm includes a sequence of (i) change detection, (ii) change characterization, (iii) region growing and (iv) attribution steps (<http://wald.anu.edu.au/challenges/bushfires/burn-mapping/>, last accessed February 2019).

6.3. Validation of BA products

The prolific advances in BA mapping methods described in the previous sections lead to a great variety of publicly available BA products. Their accuracy is inevitably a function of the characteristics of input data (e.g. optical reflectance observations) and BA retrieval algorithms. Therefore, product accuracies can vary greatly. The goal of validation is to quantify the accuracy of data products and is a direct way to inform end-users about their quality. Validation is “the process of assessing, by independent means, the quality of the data products derived from the system outputs” as defined by The Committee on Earth

Observing Satellites Working Group on Calibration and Validation (<http://lpvs.gsfc.nasa.gov/> last accessed January 2019). Accuracy is typically inferred at the scale of study from a sample of reference data.

Coarse resolution BA products have been often validated by comparing them with medium resolution data (Landsat-TM, SPOT-HRV or Sentinel-2 imagery). The Committee on Earth Observing Satellites (CEOS) Land Product Validation team ([Boschetti et al., 2009](#)) recommends that reference fire perimeters be derived from a multi-temporal pair of images to properly date the validation period. The reference sites should be properly documented (with standard metadata), discriminating between burned, unburned and unobserved data (either from clouds or technical issues).

The sampling design is critical to make the most out of the reference data. Probability sampling designs ensure that accuracy inferences are possible at global scale. The earliest BA product releases were published along with validation analyses based on selective sampling of a few test sites ([Tansey et al., 2004a, 2004b](#); [Roy et al., 2005](#)). Therefore, global accuracy inferences were not available (or they had no statistical meaning). Globcarbon ([Plummer et al., 2006](#)) and L3JRC ([Tansey et al., 2008](#)) were validated with independent data derived from 72 Landsat scenes globally distributed mostly from the year 2000. [Roy and Boschetti \(2009\)](#) reported validation results for the MCD45A1 product using a set of 11 Landsat scenes distributed across southern Africa. [Chuvieco et al. \(2008\)](#) validated a regional product for Latin America using 19 Landsat scenes and 9 China–Brazil Earth Resources Satellite (CBERS) scenes. The MCD64A1 collection 5 data were not formally validated, but some quantification of uncertainty was provided ([Giglio et al., 2009](#); [Giglio et al., 2010](#)). The most recent MCD64A1 c6 products were validated by using a set of 108 Landsat scenes distributed across a wide range of fire-affected ecosystems ([Giglio et al., 2018](#)).

After the public release of the Landsat archive, the availability of reference images was no longer a limiting factor to use probability sampling designs. The first inferences of global product accuracies became available a few years ago ([Padilla et al., 2014](#); [Padilla et al., 2015](#)). A great deal of attention was placed on (1) the definition of sampling units, by attributing them with spatial and temporal dimensions so that accuracy inferences could be made for specific spatial and temporal extents ([Boschetti et al., 2016](#)), and (2) the improvement of the efficiency of sampling designs in order to obtain as precise accuracy inferences as possible given a sample size ([Padilla et al., 2017](#)).

The first global product accuracy inferences ([Padilla et al., 2014](#); [Padilla et al., 2015](#)) were probably lower than expected and even to some extent controversial among the BA algorithm development community. The commission and omission error rates of the most accurate product were 42% and 68%, respectively ([Padilla et al., 2015](#)). Recent improvements in input data (higher spatial resolution) are leading to an important increase in accuracy ([Roteta et al., 2019](#)). Ideally, any improvement of BA products should be tracked by validation analyses, which should be externalized from algorithm developers and performed by joint initiatives including competing agencies, thus ensuring the independence that any validation should have.

If validation protocols require using higher spatial resolution images, validation of BA products generated from Landsat and similar resolution imagery can be challenging. Few image sources that have finer resolution than Landsat and are consistently collected as an alternative ([Vanderhoof et al., 2017a](#)). Now, commercial high-spatial and temporal resolution satellite imagery (such as Planet's or Geoimage's) can be acquired for statistically selected validation areas, although costs may be high. However, limited availability of historical high-resolution imagery may challenge sampling designs for validating time series of those medium-resolution BA products. Practitioners are often left with what imagery is available. Consequently, validating BA products derived from Landsat data and that span the length of the Landsat archive must also rely on Landsat-derived reference data that are independent of the Landsat data used to train the algorithm ([Vanderhoof et al., 2017b](#)). To further complicate matters, validation of the Landsat BA

products with high resolution and Landsat reference imagery can give conflicting results. For example, when using high-resolution reference imagery, BAECV (Hawbaker et al., 2017) omission and commission errors were 22% and 48%, respectively (Vanderhoof et al., 2017a). However, omission and commission of the BAECV products were 42% and 33% when validated with Landsat reference imagery (Vanderhoof et al., 2017b). The increase in commission error was largely the result of differences in resolution, as unburned areas within-fire patches could be delineated with more detail in the high-resolution imagery. However, both analyses showed that the commission and omission errors of the Landsat burned area products were less than those reported for coarse-resolution global products.

7. The way ahead

Remote sensing of burned areas has changed our view of patterns of burning and understanding of the drivers and impacts of fires at regional, continental, and global scales. Although many national, state, and local government agencies collect information about prescribed fires and wildfires, they are often error prone, incomplete, and limited because of inconsistent collection efforts over space and time, introducing much uncertainty into analyses based upon them. In contrast, the routine collection of BA data from remotely sensed imagery has allowed us to overcome many of those limitations. By applying BA detection algorithms over large spatial extents and over extended time periods, remote sensing has allowed us to generate data products that have spatial and temporal consistency, which agency reports generally lack. This includes the spatial extent of BA (perimeters), as well as within-fire heterogeneity such as identification of unburned islands within the perimeters and, in some cases, estimates of burn severity. Furthermore, the spatial progression of fires can be tracked by sensors collecting data at high temporal frequencies (e.g. daily or better). Such information has provided the foundation for national- and global-scale studies on the patterns, drivers, and impacts of fires on human and natural systems.

Chief among the strengths of existing operational BA products are their broad spatial coverage (generally global) and the comparatively long BA time series they provide (19 years in the case of those produced using MODIS data), even though the temporal sequence is still short for characterizing fire regimes and for atmospheric and carbon modelers. The most significant limitation of the existing suite of global BA products is their relatively coarse native spatial resolution, which varies from 250 m (FireCCI50) to 1 km (e.g., L3JRC). The degree of fidelity provided by such resolutions is generally not adequate for resolving small and/or highly fragmented fires (Eva and Lambin, 1998; Laris, 2005; Roy and Boschetti, 2009), leading to a substantial underreporting of BA (Padilla et al., 2015; Roteta et al., 2019). BA may also be missed when fires leave little residual heat and spread rapidly between satellite overpasses (Hawbaker et al., 2008) or when the differences between pre- and post-fire spectral characteristics are minimal. Commission errors may occur when there is confusion between BA and other disturbances, for example clear cuts, land conversion, non-fire forest mortality (Kennedy et al., 2010; Schroeder et al., 2017; Zhao et al., 2015). Given these challenges, it is not surprising that estimates of BA may vary substantially when detected with different sensors (Padilla et al., 2015) or different algorithms (Hawbaker et al., 2017).

BA products incorporate different auxiliary variables that help end users, particularly climate modelers. The uncertainty of detection is a critical one, which still needs to be better standardized, as currently it is based on algorithm-dependent approaches. The temporal reporting uncertainty should also be delivered, particularly for atmospheric modelers. The type of burned land cover generally relies on external land cover products, which obviously imply a certain degree of uncertainty on their own, further complicating the global assessment of uncertainties in final BA products.

Another limitation of current BA products is the lack of information

on combustion completeness and fraction of burned area, which are two critical parameters for atmospheric emission estimations. The combined use of BA and active fire information, both from geo-stationary and polar orbiting platforms, should benefit the current emission estimates greatly, by integrating energy release by active fires with magnitude of reflectance changes in optical images. This is particularly the case of detection of small fires, and a good representation of the temporal evolution of fires for which active fire detections provide the most information—especially from geostationary platforms. Reliable temporal information is mostly needed to align emissions with the proper atmospheric conditions for transport which is highly variable due to changing weather patterns. The key hurdle to overcome is a dearth of field measurements of fuel consumption (van Leeuwen et al., 2014). Even though Fire Radiative Power (FRP) or Fire Radiative Energy (FRE) values derived from satellite observations provide independent estimates of emissions or fuel consumption, further efforts are required to reduce the uncertainties in estimating both (Andela et al., 2016; Ichoku and Ellison, 2014; Kaiser et al., 2012).

The importance of small and/or fragmented fires for improving the estimations of atmospheric emissions and for analyzing the impacts of fire on deforestation processes is creating the momentum to undertake the generation of global BA products based on medium resolution sensors, now in the range of 10–30 m (Roteta et al., 2019). This obviously implies a high demand in terms of computer processing and data distribution and assessment, particularly for climate modelers who work at much coarser spatial resolution. Long-term regional BA products are available at much finer spatial resolution, such as the 30-m MTBS dataset, which spans the United States, though these come at a cost of reduced spatial coverage. Improvements in cloud processing and distributed archive facilities (e.g. Google Earth Engine) may greatly help to carry out global analysis at medium spatial resolution. Temporal coverage of these sensors may also create difficulties to detect fires in areas with frequent cloud cover and rapid vegetation regrowth (Hawbaker et al., 2017; Padilla et al., 2015).

The combined use of optical and SAR data may help the BA detection in regions where optical sensors perform poorly on their own. The launch of ESA's Sentinel-1 satellite constellation overcomes some of the past limitations of SAR data for BA mapping, particularly in terms of temporal coverage. Improvements in sensors characteristics (e.g., dual polarization, increased spatial resolution and incidence angle, precise orbital information), provides an excellent opportunity to develop algorithms for mapping fire impacts at continental to global scales (Engelbrecht et al., 2017; Lohberger et al., 2018; Verhegghen et al., 2016). Future research should focus on automatic, locally adaptive detection algorithms that take into account the large variability of post-fire backscatter response between vegetation types as well as variability induced by meteorological conditions during data acquisition or topographic slope.

Progress in the development of new sensors next to the rapid progress on image processing and numerical processing capabilities provide a bright future to the remote sensing applications for BA mapping in near real time, while allowing for the creation of comprehensive archives of data on BA from local to global scales. The main challenge in the operational use of medium spatial resolution imagery remains in the real-time access to the data, the timely creation of BA products through the integration of EO products of diverse sources and spatial resolutions, and their provision via web services to the final users. Wildfire management services are among the users' communities that are better adapted to use satellite products, which are often available through stable regional information systems such as the EFFIS in Europe, the Geospatial Technology and Applications Center (GTAC) in the USA or the Advance Fire Information System (AFIS) in South Africa. Although global BA products have already been available for some time, their use by operational wildfire management organizations has been fairly limited. These products were used by the modeler's communities or in the multi-annual assessment of fire effects by either

researchers or United Nations agencies such as United Nations Food and Agriculture Organization (FAO). However, the development of new initiatives such as the Global Wildfire Information System in the context of the Group on Earth Observations work program and the Copernicus European Union Program may be a catalyst for the operational use of

BA products and other EO products that may help in the management of wildfires and the assessment of wildfire impacts at the global scale.

Disclaimer: Any use of trade, product, or firm names is for descriptive purposes only and does not imply endorsement by the U.S. Government.

Annex A. List of acronyms

| Acronym | Definition |
|------------|---|
| AFIS | Advance Fire Information System |
| AR | Assessment Reports |
| ATSR | Along track scanning radiometer |
| AVHRR | Advanced Very High-Resolution Radiometer |
| BA | Burned area |
| BAECV | Burned Area Essential Climate Variable |
| BAECV | Landsat Burned Area Essential Climate Variable |
| BAI | Burned area index |
| BAIM | Modified burned area index |
| BRDF | Bidirectional reflectance distribution function |
| BFAST | Breaks for Additive Seasonal and Trend |
| BGR | Blue, green and red |
| CBI | Composite Burned Index |
| CCI | Climate Change Initiative |
| CCM | Chemistry–climate models |
| CEOS | Committee on Earth Observing Satellites |
| CONABIO | Comisión Nacional para el Conocimiento y Uso de la Biodiversidad |
| COP | Conference of the Parties |
| CTM | Chemical transport models |
| CWFIS | Canadian Wildland Fire Information System |
| DGVM | Dynamic Global Vegetation Model |
| EFFIS | European Forest Fire Information System |
| EMS | Emergency Management Service |
| EMT + | Enhanced Thematic Mapper Plus |
| Envisat | Environmental satellite |
| EO | Earth observation |
| ERS | European Remote-Sensing Satellite |
| ERTS | Earth Resources Technology Satellite |
| ESA | European Space Agency |
| EUSF | European Union Solidarity Fund |
| FAO | Food and Agriculture Organization |
| FINN | Fire INventory from NCAR |
| FireCCI50 | MODIS based 250 m global BA product derived from the Fire_cci project |
| FOFEM | First-Order Fire Effects Model |
| FRE | Fire Radiative Energy |
| FRP | Fire radiative power |
| GA | Geoscience Australia |
| GBA | Global Burnt Area |
| GCOS | Global Climate Observing System |
| GDP | Global domestic product |
| GEMI | Global environmental monitoring index |
| GFED | Global Fire Emission Database |
| GIO_GL1 | Global BA product derived from the Copernicus Land Service |
| GIS | Geographic information systems |
| GLAS | Geoscience Laser Altimeter System |
| GLOBSCAR | Global Burn Scars |
| HH | Horizontal-horizontal |
| HRV | Haute Résolution Visible |
| HRV | High Resolution Visibl |
| HS | Hotspots |
| HV | Horizontal-vertical |
| ICESat | Ice, Cloud, and land Elevation Satellite |
| InSAR | Interferometric synthetic aperture radar |
| IPCC | Intergovernmental Panel on Climate Change |
| IRS | Indian Remote Sensing |
| Landsat | Land Remote-Sensing Satellite |
| LandTrendr | Trends in Disturbance and Recovery |
| Lidar | Light Detection and Ranging |
| LISS | Linear imaging and self-scanning sensor |
| LTDR | Long Term Data Record |
| M3 | Monitoring, mapping and modeling |
| MERIS | MEdium Resolution Imaging Spectrometer |
| MESMA | Multiple Endmember Spectral Mixture Analysis |
| MIR | Middle infrared |
| MIRBI | Mid-infrared burn index |
| MODIS | Moderate Resolution Imaging Spectroradiometer |
| MSI | Multispectral Instrument |

| | |
|---------|---|
| MSS | Multispectral scanner |
| MTBS | Monitoring Trends in Burn Severity |
| NAFI | North Australia and Rangelands Fire Information |
| NASA | National Aeronautics and Space Administration |
| NBR | Normalized burned ratio |
| NCAR | National Center for Atmospheric Research |
| NDMI | Normalized Difference Moisture Index |
| NDVI | Normalized difference vegetation index |
| NDWI | Normalized Difference Water Index |
| NIR | Near infrared |
| NOAA | National Oceanographic and Atmospheric Administration |
| NOFFi | National Observatory of Forest Fires |
| NRT | Near real time |
| OBAM | Operational Burned Area Mapping |
| OBIA | Object-based image analysis |
| OLI | Operational Land Imager |
| PAL | Pathfinder AVHRR Land product |
| PCA | Principal component analysis |
| PROBA-V | Project for On-Board Autonomy Vegetation |
| Radar | Radio detection and ranging |
| RSAC | Remote Sensing Applications Center |
| RTM | Radiative transfer models |
| SAR | Synthetic aperture radar |
| SAVI | Soil Adjusted Vegetation Index |
| SDG | Sustainable Development Goals |
| SMA | Spectral mixture analysis |
| SPOT | Système Probatoire d'Observation de la Terre |
| SVM | Support vector machines |
| SWIR | Short-wave infrared |
| TIR | Thermal infrared |
| TM | Thematic Mapper |
| USGS | United States Geological Survey |
| VCT | Vegetation Change Tracker |
| VGT | VEGETATION instrument |
| VH | Vertical-horizontal |
| VV | Vertical-vertical |
| WFLC | Wildland Fire Leadership Council |
| WIFS | Wide field sensor |

References

- Ahern, F.J., Goldammer, J.G., Justice, C.O. (Eds.), 2001. *Global and Regional Vegetation Fire Monitoring From Space: Planning a Coordinated International Effort*. SPB Academic Publishing, The Hague, The Netherlands.
- Alonso-Canas, I., Chuvieco, E., 2015. Global burned area mapping from ENVISAT-MERIS data. *Remote Sens. Environ.* 163, 140–152.
- Alonzo, M., Morton, D.C., Cook, B.D., Andersen, H., Babcock, C., Pattison, R., 2017. Patterns of canopy and surface layer consumption in a boreal forest fire from repeat airborne lidar. *Environ. Res. Lett.* 12, 065004.
- Ambrosia, V.G., Brass, J.A., 1988. Thermal analysis of wildfires and effects on global ecosystem cycling. *Geocarto Int.* 1, 29–39.
- Andela, N., van der Werf, G.R., Kaiser, J.W., van Leeuwen, T.T., Wooster, M.J., Lehmann, C.E.R., 2016. Biomass burning fuel consumption dynamics in the tropics and subtropics assessed from satellite. *Biogeosciences* 13, 3717–3734.
- Andela, N., Morton, D.C., Giglio, L., Chen, Y., van der Werf, G.R., Kasibhatla, P.S., DeFries, R.S., Collatz, G.J., Hantson, S., Kloster, S., Bachelet, D., Forrest, M., Lasslop, G., Li, F., Mangleon, S., Melton, J.R., Yue, C., Randerson, J.T., 2017. A human-driven decline in global burned area. *Science* 356, 1356–1362.
- Archibald, S., Roy, D.P., B., V.W., & J., S.R., 2009. What limits fire? An examination of drivers of burnt area in Southern Africa. *Glob. Chang. Biol.* 15, 613–630.
- Asrar, G., Harris, T.R., Lapitan, R.L., Cooper, D.I., 1988. Radiative surface temperatures of the burned and unburned areas in a Tallgrass Prairie. *Remote Sens. Environ.* 24, 447–457.
- Ballhorn, U., Siegert, F., Mason, M., Limin, S., 2009. Derivation of burn scar depths and estimation of carbon emissions with LIDAR in Indonesian peatlands. *Proc. Natl. Acad. Sci.* 106, 21213.
- Barbosa, P.M., Grégoire, J.M., Pereira, J.M.C., 1999a. An algorithm for extracting burned areas from time series of AVHRR GAC data applied at a continental scale. *Remote Sens. Environ.* 69, 253–263.
- Barbosa, P.M., Stroppiana, D., Grégoire, J.M., Pereira, J.M.C., 1999b. An assessment of vegetation fire in Africa (1981–1991): burned areas, burned biomass, and atmospheric emissions. *Glob. Biogeochem. Cycles* 13, 933–950.
- Barros, A.M.G., Pereira, J.M.C., 2014. Wildfire selectivity for land cover types: does size matter? *PLoS One* 9 (1), e84760.
- Bastarrika, A., Chuvieco, E., Martín, M.P., 2011a. Automatic burned land mapping from MODIS time series images: assessment in Mediterranean ecosystems. *IEEE Trans. Geosci. Remote Sens.* 49, 3401–3413.
- Bastarrika, A., Chuvieco, E., Martín, M.P., 2011b. Mapping burned areas from Landsat TM/ETM+ data with a two-phase algorithm: balancing omission and commission errors. *Remote Sens. Environ.* 115, 1003–1012.
- Benz, U.C., Hofmann, P., Willhauck, G., Lingenfelder, I., Heynen, M., 2004. Multi-resolution, object-oriented fuzzy analysis of remote sensing data for GIS-ready information. *ISPRS J. Photogramm. Remote Sens.* 58, 239–258.
- Birk, E.M., Simpson, R., 1980. Steady state and the continuous input model of litter accumulation and decomposition in Australian eucalypt forests. *Ecology* 61, 481–485.
- Bistinas, I., Harrison, S., Prentice, I.C., Pereira, J., 2014. Causal relationships versus emergent patterns in the global controls of fire frequency. *Biogeosciences* 11, 5087–5101.
- Boschetti, L., Brivio, P.A., Gregoire, J.M., 2003. The use of Meteosat and GMS imagery to detect burned areas in tropical environments. *Remote Sens. Environ.* 85, 78–91.
- Boschetti, L., Roy, D.P., Justice, C.O., 2009. *International Global Burned Area Satellite Product Validation Protocol. Part I – Production and Standardization of Validation Reference Data*. http://lpvs.gsfc.nasa.gov/DOC/protocol_revised_Apr09.doc.
- Boschetti, L., Roy, D.P., Justice, C.O., Humber, M.L., 2015. MODIS–Landsat fusion for large area 30 m burned area mapping. *Remote Sens. Environ.* 161, 27–42.
- Boschetti, L., Stehman, S.V., Roy, D.P., 2016. A stratified random sampling design in space and time for regional to global scale burned area product validation. *Remote Sens. Environ.* 186, 465–478.
- Bourgeau-Chavez, L.L., Kasischke, E.S., French, N.H.F., Szeto, L.H., Kherkher, C.M., 1994. Using ERS-1 SAR imagery to monitor variations in burn severity in an Alaskan fire-disturbed boreal forest ecosystem. In: *Geoscience and Remote Sensing Symposium, 1994. IGARSS '04. Proceedings. IEEE International, Pasadena, California*, pp. 243–245.
- Bourgeau-Chavez, L.L., Harrell, P.A., Kasischke, E.S., French, H.F., 1997. The detection and mapping of Alaskan wildfires using a spaceborne imaging radar system. *Int. J. Remote Sens.* 18, 355–373.
- Bourgeau-Chavez, L.L., Kasischke, E.S., Brunzell, S., Mudd, J.P., 2002. Mapping fire scars in global boreal forests using imaging radar data. *Int. J. Remote Sens.* 23, 4211–4234.
- Bowman, D.M.J.S., Balch, J.K., Artaxo, P., Bond, W.J., Carlson, J.M., Cochrane, M.A., D'Antonio, C.M., DeFries, R.S., Doyle, J.C., Harrison, S.P., Johnston, F.H., Keeley, J.E., Krawchuk, M.A., Kull, C.A., Marston, J.B., Moritz, M.A., Prentice, I.C., Roos, C., Scott, A., Swetnam, T., Van der Werf, G., Pyne, S.J., 2009. Fire in the Earth system. *Science* 324, 481–484.
- Bowman, D.M., Williamson, G.J., Abatzoglou, J.T., Kolden, C.A., Cochrane, M.A., Smith, A.M., 2017. Human exposure and sensitivity to globally extreme wildfire events. *Nat. Ecol. Evol.* 1, 0058.
- Brewer, C.K., Winne, J.C., Redmond, R.L., Opitz, D.W., Mangrich, M.V., 2005. Classifying and mapping wildfire severity: a comparison of methods. *Photogramm. Eng. Remote Sens.* 71, 1311–1320.
- Brooks, E.B., Wynne, R.H., Thomas, V.A., Blinn, C.E., Coulston, J.W., 2014. On-the-fly massively multitemporal change detection using statistical quality control charts and Landsat data. *IEEE Trans. Geosci. Remote Sens.* 52, 3316–3332.

- Caetano, M.S., Mertes, L.A.K., Cadete, L., Pereira, J.M.C., 1996. Assessment of AVHRR data for characterizing burned areas and post-fire vegetation recovery. *EARSel Adv. Remote Sens.* 4, 124–134.
- Cahoon, D.R., Stocks, B.J., Levine, J.S., Cofer, W.R., Chung, C.C., 1992. Evaluation of a technique for satellite-derived area estimation of forest fires. *J. Geophys. Res.* 97, 3805–3814.
- Cahoon, D.R., Stocks, B.J., Levine, J.S., Cofer, W.R., Pierson, J.M., 1994. Satellite analysis of the severe 1987 forest fires in Northern China and Southeastern Siberia. *J. Geophys. Res.* 99, 18627–18638.
- Cao, X., Chen, J., Imura, H., Higashi, O., 2009. A SVM-based method to extract urban areas from DMSP-OLS and SPOT VGT data. *Remote Sens. Environ.* 113, 2205–2209.
- Carmona-Moreno, C., Belward, A., Malingreau, J.P., Hartley, A., Garcia-Alegre, M., Antonovskiy, M., Buchshtaber, V., Pivovarov, V., 2005. Characterizing interannual variations in global fire calendar using data from Earth observing satellites. *Glob. Chang. Biol.* 11, 1537–1555.
- Cascio, W.E., 2018. Wildland fire smoke and human health. *Sci. Total Environ.* 624, 586–595.
- Caughlin, T.T., Elliott, S., Lichstein, J.W., 2016. When does seed limitation matter for scaling up reforestation from patches to landscapes? *Ecol. Appl.* 26 (8), 2437–2448.
- Ceccato, P., Flasse, S., Tarantola, S., Jacquemoud, S., Grégoire, J.M., 2001. Detecting vegetation leaf water content using reflectance in the optical domain. *Remote Sens. Environ.* 77, 22–33.
- Chu, T., Guo, X., 2014. Remote sensing techniques in monitoring post-fire effects and patterns of forest recovery in boreal Forest regions: a review. *Remote Sens.* 6, 470.
- Chuvieco, E., Congalton, R.G., 1988. Mapping and inventory of forest fires from digital processing of TM data. *Geocarto Int.* 4, 41–53.
- Chuvieco, E., Martín, M.P., 1994a. Global fire mapping and fire danger estimation using AVHRR images. *Photogramm. Eng. Remote. Sens.* 60, 563–570.
- Chuvieco, E., Martín, M.P., 1994b. A simple method for fire growth mapping using AVHRR channel 3 data. *Int. J. Remote Sens.* 15, 3141–3146.
- Chuvieco, E., Martín, M.P., Palacios, A., 2002. Assessment of different spectral indices in the red-near-infrared spectral domain for burned land discrimination. *Int. J. Remote Sens.* 23, 5103–5110.
- Chuvieco, E., Riaño, D., Danson, F.M., Martín, M.P., 2006. Use of a radiative transfer model to simulate the post-fire spectral response to burn severity. *J. Geophys. Res. Biogeosci.* 111. <https://doi.org/10.1029/2005JG000143>.
- Chuvieco, E., Opazo, S., Stone, W., Del Valle, H., Anaya, J., Di Bella, C., Cruz, I., Manzo, L., López, G., Mari, N., González-Alonso, F., Morelli, F., Setzer, A., Csizsar, I., Kanpandegi, J.A., Bastarrrika, A., Libonati, R., 2008. Global burned land estimation in Latin America using MODIS composite data. *Ecol. Appl.* 18, 64–79.
- Chuvieco, E., Aguado, I., Yebra, M., Nieto, H., Salas, J., Martín, P., Vilar, L., Martínez, J., Martín, S., Ibarra, P., de la Riva, J., Baeza, J., Rodríguez, F., Molina, J.R., Herrera, M.A., Zamora, R., 2010. Development of a framework for fire risk assessment using remote sensing and geographic information system technologies. *Ecol. Model.* 221, 46–58.
- Chuvieco, E., Martínez, S., Roman, M.V., Hantson, S., Pettinari, L., 2014. Integration of ecological and socio-economic factors to assess global wildfire vulnerability. *Glob. Ecol. Biogeogr.* 23, 245–258.
- Chuvieco, E., Yue, C., Heil, A., Mouillot, F., Alonso-Canas, I., Padilla, M., Pereira, J.M., Oom, D., Tansey, K., 2016. A new global burned area product for climate assessment of fire impacts. *Glob. Ecol. Biogeogr.* 25, 619–629.
- Chuvieco, E., Lizundia-Loiola, J., Pettinari, M.L., Ramo, R., Padilla, M., Tansey, K., Mouillot, F., Laurent, P., Storm, T., Heil, A., Plummer, S., 2018. Generation and analysis of a new global burned area product based on MODIS 250 m reflectance bands and thermal anomalies. *Earth Syst. Sci. Data Discuss.* 2018, 1–24.
- Cochrane, M.A., Alencar, A., Schulze, M.D., Souza, C.M., Nepstad, D.C., Lefebvre, P., Davidson, E.A., 1999. Positive feedbacks in the fire dynamic of closed canopy tropical forests. *Science* 284, 1832–1835.
- Cohen, W.B., Yang, Z., Kennedy, R., 2010. Detecting trends in forest disturbance and recovery using yearly Landsat time series: 2. TimeSync — tools for calibration and validation. *Remote Sens. Environ.* 114, 2911–2924.
- Cohen, W.B., Yang, Z., Healey, S.P., Kennedy, R.E., Gorelick, N., 2018. A LandTrendr multispectral ensemble for forest disturbance detection. *Remote Sens. Environ.* 205, 131–140.
- Daniau, A.-L., Sánchez Goñi, M.F., Martínez, P., Urrego, D.H., Bout-Roumzeilles, V., Desprat, S., Marlon, J.R., 2013. Orbital-scale climate forcing of grassland burning in southern Africa. *Proc. Natl. Acad. Sci.* 110, 5069–5073.
- De Santis, A., Chuvieco, E., 2007. Burn severity estimation from remotely sensed data: performance of simulation versus empirical models. *Remote Sens. Environ.* 108, 422–435.
- De Santis, A., Chuvieco, E., Vaughan, P., 2009. Short-term assessment of burn severity using the inversion of PROSPECT and GeoSail models. *Remote Sens. Environ.* 113, 126–136.
- De Santis, A., Asner, G.P., Vaughan, P.J., Knapp, D.E., 2010. Mapping burn severity and burning efficiency in California using simulation models and Landsat imagery. *Remote Sens. Environ.* 114, 1535–1545.
- van der Werf, G.R., Randerson, J.T., Collatz, G.J., Giglio, L., 2003. Carbon emissions from fires in tropical and subtropical ecosystems. *Glob. Chang. Biol.* 9 (4), 547–562.
- van der Werf, G.R., Randerson, J.T., Collatz, G.J., Giglio, L., Kasibhatla, P.S., Arellano, A.F., Olsen, S.C., Kasischke, E.S., 2004. Continental-scale partitioning of fire emissions during the 1997 to 2001 El Niño/La Niña period. *Science* 303 (5654), 73–76.
- van der Werf, G.R., Randerson, J.T., Giglio, L., Collatz, G.J., Kasibhatla, P.S., Arellano, A.F., 2006. Interannual variability in global biomass burning emissions from 1997 to 2004. *Atmos. Chem. Phys.* 6, 3423–3441.
- van der Werf, G.R., Randerson, J.T., Giglio, L., Collatz, G., Mu, M., Kasibhatla, P.S., Morton, D.C., DeFries, R.S., Jin, Y., van Leeuwen, T.T., 2010. Global fire emissions and the contribution of deforestation, savanna, forest, agricultural, and peat fires (1997–2009). *Atmos. Chem. Phys.* 10, 11707–11735.
- van der Werf, G.R., Randerson, J.T., Giglio, L., van Leeuwen, T.T., Chen, Y., Rogers, B.M., Mu, M., van Marle, M.J.E., Morton, D.C., Collatz, G.J., Yokelson, R.J., Kasibhatla, P.S., 2017. Global fire emissions estimates during 1997–2016. *Earth Syst. Sci. Data* 9, 697–720.
- DeVries, B., Verbesselt, J., Kooistra, L., Herold, M., 2015. Robust monitoring of small-scale forest disturbances in a tropical montane forest using Landsat time series. *Remote Sens. Environ.* 161, 107–121.
- Dobson, M.C., Ulaby, T., Le Toan, T., Beaudoin, A., Kasischke, E.S., 1992. Dependence of radar backscatter on coniferous forest biomass. *IEEE Trans. Geosci. Remote Sens.* 30, 412–415.
- Doerr, S.H., Shakesby, R.A., Blake, W.H., Chafer, C.J., Humphreys, G.S., Wallbrink, P.J., 2006. Effects of differing wildfire severities on soil wettability and implications for hydrological response. *J. Hydrol.* 319, 295–311.
- Dragozi, E., Gitas, I., Stavrakoudis, D., Theocharis, J., 2014. Burned area mapping using support vector machines and the FuzCoC feature selection method on VHR IKONOS imagery. *Remote Sens.* 6, 12005–12036.
- Duncan, R.S., Duncan, V.E., 2000. Forest succession and distance from forest edge in an afro tropical grassland. *Biotropica* 32 (1), 33–41.
- Duncan, B.N., Martin, R.V., Staudt, A.C., Yevich, R., Logan, J.A., 2003. Interannual and seasonal variability of biomass burning emissions constrained by satellite observations. *J. Geophys. Res.* 108 (D2), 4040. <https://doi.org/10.1029/2002JD002378>.
- Dwyer, E., Pereira, J.M.C., Grégoire, J.-M., DaCamara, C.C., 2000a. Characterization of the spatio-temporal patterns of global fire activity using satellite imagery for the period April 1992 to March 1993. *J. Biogeogr.* 27, 57–69.
- Dwyer, E., Pinnock, S., Grégoire, J.-M., Pereira, J.M.C., 2000b. Global spatial and temporal distribution of vegetation fire as determined from satellite observations. *Int. J. Remote Sens.* 21, 1289–1302.
- Eastwood, J.A., Plummer, S.E., Wyatt, B.K., Stocks, B.J., 1998. The potential of SPOT-vegetation data for fire scar detection in boreal forests. *Int. J. Remote Sens.* 19, 3681–3687.
- Eidenshink, J., Schwind, B., Brewer, K., Zhu, Z.-L., Quayle, B., Howard, S., 2007. A project for monitoring trends in burn severity. *Fire Ecol.* 3, 3–21.
- Engelbrecht, J., Theron, A., Vhengani, L., Ke, J., 2017. A simple normalized difference approach to burnt area mapping using multi-polarisation C-band SAR. *Remote Sens.* 9, 764.
- Eva, H., Lambin, E.F., 1998. Burnt area mapping in Central Africa using ATSR data. *Int. J. Remote Sens.* 19, 3473–3497.
- Fearnside, P.M., Lima de Alencastro Graça, P.M., Alves Rodriguez, F.J., 2001. Burning of Amazonian rainforests: burning efficiency and charcoal formation in forest cleared for cattle pasture near Manaus, Brazil. *For. Ecol. Manag.* 146, 115–128.
- Fernández, A., Illera, P., Casanova, J.L., 1997. Automatic mapping of surfaces affected by forest fires in Spain using AVHRR NDVI composite image data. *Remote Sens. Environ.* 60, 153–162.
- Fernandez-Manso, A., Quintano, C., Roberts, D.A., 2016. Burn severity influence on post-fire vegetation cover resilience from Landsat MESMA fraction images time series in Mediterranean forest ecosystems. *Remote Sens. Environ.* 184, 112–123.
- Flannigan, M.D., Vonder Haar, T.H., 1986. Forest fire monitoring using NOAA satellite AVHRR. *Can. J. For. Res.* 16, 975–982.
- Flasse, S.P., Ceccato, P., 1996. A contextual algorithm for AVHRR fire detection. *Int. J. Remote Sens.* 17, 419–424.
- Forkel, M., Andela, N., Harrison, S.P., Lasslop, G., van Marle, M., Chuvieco, E., Dorigo, W., Forrest, M., Hantson, S., Heil, A., Li, F., Melton, J., Sitch, S., Yue, C., Arneeth, A., 2019. Emergent relationships on burned area in global satellite observations and fire-enabled vegetation models. *Biogeosciences* 16, 47–76.
- Fraser, R.H., Li, Z., Cihlar, J., 2000. Hotspot and NDVI Differencing Synergy (HANDS): a new technique for burned area mapping over boreal forest. *Remote Sens. Environ.* 74, 362–376.
- Fraser, R.H., Hall, R.J., Landry, R., Lynham, T., Raymond, D., Lee, B., Li, Z., 2004. Validation and calibration of Canada-wide coarse-resolution satellite burned-area maps. *Photogramm. Eng. Remote. Sens.* 70, 451–460.
- French, N.H., Kasischke, E.S., Hall, R.J., Murphy, K.A., Verbyla, D.L., Hoy, E.E., Allen, J.L., 2008. Using Landsat data to assess fire and burn severity in the North American boreal forest region: an overview and summary of results. *Int. J. Wildland Fire* 17, 443–462.
- Fuller, S.P., Rouse, W.R., 1979. Spectral reflectance changes accompanying a post-fire recovery sequence in a subarctic spruce-lichen woodland. *Remote Sens. Environ.* 8, 11–23.
- Furyaev, V.V., 1985. The use of aerospace imagery to examine and assess the consequences of forest fires. *Sov. J. Remote. Sens.* 4, 773–782.
- Furyaev, V.V., Kireev, D.M., Sukhikh, V.I., Zhirin, V.M., 1985. Space imagery application to assess forest disturbance by fires. *Sov. J. Remote. Sens.* 3, 226–234.
- García, M., Saatchi, S., Casas, A., Koltunov, A., Ustin, S., Ramirez, C., Garcia-Gutierrez, J., Baltzer, H., 2017. Quantifying biomass consumption and carbon release from the California Rim fire by integrating airborne LiDAR and Landsat OLI data. *J. Geophys. Res. Biogeosci.* 122, 340–353.
- García-Haro, F.J., Gilbert, M.A., Meliá, J., 2001. Monitoring fire-affected areas using Thematic Mapper data. *Int. J. Remote Sens.* 22, 533–549.
- GCOS, 2016. The Global Observing System for Climate: Implementation Needs. GCOS-200. World Meteorological Organization, Geneva, Switzerland.
- Giglio, L., Desclotres, J., Justice, C.O., Kaufman, Y.J., 2003. An Enhanced Contextual Fire Detection Algorithm for MODIS. *Remote Sens. Environ.* 87, 273–282.
- Giglio, L., Csizsar, I., Justice, C.O., 2006. Global distribution and seasonality of active fires as observed with the Terra and Aqua Moderate Resolution Imaging Spectroradiometer (MODIS) sensors. *J. Geophys. Res. Biogeosci.* 111. <https://doi.org/10.1029/2005JG000143>.

- org/10.1029/2005JG000142.
- Giglio, L., Loboda, T., Roy, D.P., Quayle, B., Justice, C.O., 2009. An active-fire based burned area mapping algorithm for the MODIS sensor. *Remote Sens. Environ.* 113, 408–420.
- Giglio, L., Randerson, J.T., van der Werf, G.R., Kasibhatla, P.S., Collatz, G.J., Morton, D.C., DeFries, R.S., 2010. Assessing variability and long-term trends in burned area by merging multiple satellite fire products. *Biogeosciences* 7, 1171–1186.
- Giglio, L., Randerson, J.T., Werf, G.R., 2013. Analysis of daily, monthly, and annual burned area using the fourth generation global fire emissions database (GFED4). *J. Geophys. Res. Biogeosci.* 118, 317–328.
- Giglio, L., Boschetti, L., Roy, D.P., Humber, M.L., Justice, C.O., 2018. The collection 6 MODIS burned area mapping algorithm and product. *Remote Sens. Environ.* 217, 72–85.
- Gilroy, J.J., Woodcock, P., Edwards, F.A., Wheeler, C., Baptiste, B.L., Uribe, C.A.M., Haugaasen, T., Edwards, D.P., 2014. Cheap carbon and biodiversity co-benefits from forest regeneration in a hotspot of endemism. *Nat. Clim. Chang.* 4, 503–507.
- Gimeno, M., San-Miguel-Ayanz, J., 2004. Evaluation of RADARSAT-1 data for identification of burnt areas in Southern Europe. *Remote Sens. Environ.* 92, 370–375.
- Gitas, I.Z., Mitri, G.H., Ventura, G., 2004. Object-based image classification for burned area mapping of Creus Cape, Spain, using NOAA-AVHRR imagery. *Remote Sens. Environ.* 92, 409–413.
- Goetz, S.J., Sun, M., Baccini, A., Beck, P.S., 2010. Synergistic use of spaceborne lidar and optical imagery for assessing forest disturbance: an Alaska case study. *J. Geophys. Res. Biogeosci.* 115.
- Goodenough, D.G., Chen, H., Richardson, A., Cloude, S., Hong, W., Li, Y., 2011. Mapping fire scars using Radarsat-2 polarimetric SAR data. *Can. J. Remote Sens.* 37, 500–509.
- Goodwin, N.R., Collett, L.J., 2014. Development of an automated method for mapping fire history captured in Landsat TM and ETM+ time series across Queensland, Australia. *Remote Sens. Environ.* 148, 206–221.
- Grégoire, J.M., Tansey, K., Silva, J.M.N., 2003. The GBA2000 initiative: developing a global burned area database from SPOT-VEGETATION imagery. *Int. J. Remote Sens.* 24, 1369–1376.
- Gutman, G., Bartalev, S., Korovin, G., 1995. Delineation of large fire damage areas in boreal forests using NOAA-AVHRR measurements. *Adv. Space Res.* 15, 111–113.
- Hall, D.K., Ormsby, J.P., Johnson, L., Brown, J., 1980. Landsat digital analysis of the initial recovery of burned tundra at Kokolik river, Alaska. *Remote Sens. Environ.* 10, 263–272.
- Hall, J.V., Loboda, T.V., Giglio, L., McCarty, G.W., 2016. A MODIS-based burned area assessment for Russian croplands: mapping requirements and challenges. *Remote Sens. Environ.* 184, 506–521.
- Hansen, M., Egorov, A., Potapov, P., Stehman, S., Tyukavina, A., Turubanova, S., Roy, D.P., Goetz, S., Loveland, T., Ju, J., 2014. Monitoring conterminous United States (CONUS) land cover change with web-enabled Landsat data (WELD). *Remote Sens. Environ.* 140, 466–484.
- Hanson, S., Pueyo, S., Chuvieco, E., 2015. Global fire size distribution is driven by human impact and climate. *Glob. Ecol. Biogeogr.* 24, 77–86.
- Hanson, S., Arneith, A., Harrison, S.P., Kelley, D.I., Prentice, I.C., Rabin, S.S., Archibald, S., Mouillot, F., Arnold, S.R., Artaxo, P., 2016. The status and challenge of global fire modelling. *Biogeosciences* 13, 3359–3375.
- Hao, W.M., Liu, M.-H., 1994. Spatial and temporal distribution of tropical biomass burning. *Glob. Biogeochem. Cycles* 8 (4), 495–503.
- Hawbaker, T.J., Radeloff, V.C., Syphard, A.D., Zhu, Z., Stewart, S.I., 2008. Detection rates of the MODIS active fire product in the United States. *Remote Sens. Environ.* 112, 2656–2664.
- Hawbaker, T.J., Vanderhoof, M.K., Beal, Y.-J., Takacs, J.D., Schmidt, G.L., Falgout, J.T., Williams, B., Fairaux, N.M., Caldwell, M.K., Picotte, J.J., 2017. Mapping burned areas using dense time-series of Landsat data. *Remote Sens. Environ.* 198, 504–522.
- Helfert, M.R., Lulla, K.P., 1990. Mapping Continental-Scale biomass burning and smoke plumes palls over the Amazon Basin as observed from the space shuttle. *Photogramm. Eng. Remote. Sens.* 56, 1367–1373.
- Hitchcock, H., Hoffer, R., 1974. Mapping a recent forest fire with ERTS-1 MSS data. *Remote Sens. Earth Resour.* 3, 449–461.
- Hope, A.S., McDowell, T.P., 1992. The relationship between surface temperature and a spectral vegetation index of a tallgrass prairie: effects of burning and other landscape controls. *Int. J. Remote Sens.* 13, 2849–2863.
- Hu, Y., Fernandez-Anez, N., Smith, T.E., Rein, G., 2018. Review of emissions from smouldering peat fires and their contribution to regional haze episodes. *Int. J. Wildland Fire* 27, 293–312.
- Huang, S., Siegert, F., 2006. Backscatter change on fire scars in Siberian boreal forests in ENVISAT ASAR wide-swath images. *IEEE Trans. Geosci. Remote Sens. Lett.* 3, 154–158.
- Huang, C., Goward, S.N., Masek, J.G., Thomas, N., Zhu, Z., Vogelmann, J.E., 2010. An automated approach for reconstructing recent forest disturbance history using dense Landsat time series stacks. *Remote Sens. Environ.* 114, 183–198.
- Humber, M.L., Boschetti, L., Giglio, L., Justice, C.O., 2018. Spatial and temporal inter-comparison of four global burned area products. *Int. J. Digital Earth* 1–25.
- Ichoku, C., Ellison, L., 2014. Global top-down smoke-aerosol emissions estimation using satellite fire radiative power measurements. *Atmos. Chem. Phys.* 14, 6643–6667.
- Imperatore, P., Azar, R., Fabiana Cal'o, D.S., Brivio, P.A., Lanari, R., Pepe, A., 2017. Effect of the vegetation fire on backscattering: an investigation based on Sentinel-1 observations. *IEEE J. Sel. Top. Appl. Earth Observ. Remote Sens.* 10, 4478–4492.
- Isaacson, D.L., Smith, H.G., Alexander, C.J., 1982. Erosion hazard reduction in a wildfire damaged area. In: Johansson, C.J., Sanders, J.L. (Eds.), *Remote Sensing for Resource Management*. Soil Conservation Society of America, Ankeny (Iowa), pp. 179–190.
- Isaksen, I., Granier, C., Myhre, G., Bernsten, T., Dalsoren, S., Gauss, M., Klimont, Z., Benestad, R., Bousquet, P., Collins, W., 2009. Atmospheric composition change: climate–chemistry interactions. *Atmos. Environ.* 43, 5138–5192.
- Ito, A., Penner, J.E., 2004. Global estimates of biomass burning emissions based on satellite imagery for the year 2000. *J. Geophys. Res.-Atmos.* 109 (14).
- Jakubauskas, M.E., Lulla, K.P., Mausel, P.W., 1990. Assessment of vegetation change in a fire-altered forest landscape. *Photogramm. Eng. Remote. Sens.* 56, 371–377.
- Jin, Y., Randerson, J.T., Goetz, S.J., Beck, P.S., Lorant, M.M., Goulden, M.L., 2012. The influence of burn severity on postfire vegetation recovery and albedo change during early succession in North American boreal forests. *J. Geophys. Res. Biogeosci.* 117.
- Jolly, W.M., Cochrane, M.A., Freeborn, P.H., Holden, Z.A., Brown, T.J., Williamson, G.J., Bowman, D.M., 2015. Climate-induced variations in global wildfire danger from 1979 to 2013. *Nat. Commun.* 6.
- Kaiser, J., Heil, A., Andreae, M., Benedetti, A., Chubarova, N., Jones, L., Morcrette, J.-J., Razinger, M., Schultz, M., Suttie, M., 2012. Biomass burning emissions estimated with a global fire assimilation system based on observed fire radiative power. *Biogeosciences* 9, 527–554.
- Kalogirou, V., Ferrazzoli, P., Vecchia, A.D., Fomelis, M., 2014. On the SAR backscatter of burned forests: a model-based study in C-band, over burned pine canopies. *IEEE Trans. Geosci. Remote Sens.* 52, 6205–6215.
- Kane, V.R., Lutz, J.A., Cansler, C.A., Povak, N.A., Churchill, D.J., Smith, D.F., Kane, J.T., North, M.P., 2015. Water balance and topography predict fire and forest structure patterns. *For. Ecol. Manag.* 338, 1–13.
- Kasischke, E., 2000. Boreal ecosystems in the global carbon cycle. In: Kasischke, E., Stocks, B.J. (Eds.), *Fire, Climate Change and Carbon Cycling in the Boreal Forest*. Springer, New York, pp. 19–30.
- Kasischke, E., French, N.H., 1995. Locating and estimating the areal extent of wildfires in Alaskan boreal forest using multiple-season AVHRR NDVI composite data. *Remote Sens. Environ.* 51, 263–275.
- Kasischke, E.S., Bourgeau-Chavez, L.L., French, N.H.F., Harrel, P., Christensen, N.L., 1992. Initial observations on using SAR to monitor wildfire scars in boreal forest. *Int. J. Remote Sens.* 13, 3495–3501.
- Kasischke, E.S., French, N.H.F., Harrel, P., Christensen, N.L., Ustin, S.L., Barry, D., 1993. Monitoring of wildfires in Boreal Forests using large area AVHRR NDVI composite image data. *Remote Sens. Environ.* 45, 61–71.
- Kasischke, E.S., Bourgeau-Chavez, L.L., French, N.H.F., 1994. Observations of variations in ERS-1 SAR image intensity associated with forest fires in Alaska. *IEEE Trans. Geosci. Remote Sens.* 32, 206–210.
- Kasischke, E.S., Bourgeau-Chavez, L.L., Johnstone, J.F., 2007. Assessing spatial and temporal variations in surface soil moisture in fire-disturbed black spruce forests in interior Alaska using spaceborne synthetic aperture radar imagery - implications for post-fire tree recruitment. *Remote Sens. Environ.* 108, 42–58.
- Kelly, L., Brotons, L., 2017. Using fire to promote biodiversity. *Science* 355, 1264–1265.
- Kennedy, R.E., Yang, Z., Cohen, W.B., 2010. Detecting trends in forest disturbance and recovery using yearly Landsat time series: 1. LandTrendr — temporal segmentation algorithms. *Remote Sens. Environ.* 114, 2897–2910.
- Key, C., Benson, N., 1999. The Normalized Burned Ratio, a Landsat TM radiometric index of burn severity incorporating multi-temporal differencing. In: *U.S. Geological Survey*. <http://www.nrmisc.usgs.gov/research/ndbr.htm>.
- Key, C.H., Benson, N., 2006. Landscape assessment (LA). Sampling and analysis methods. In: Lutes, D.C., Keane, R.E., Caratti, J.F., Key, C.H., Benson, N.C., Sutherland, S., Gangi, L.J. (Eds.), *FIREMON: Fire effects Monitoring and Inventory System. Integration of Standardized Field Data Collection Techniques and Sampling Design With Remote Sensing to Assess Fire Effects*. U.S. Department of Agriculture, Forest Service, Rocky Mountain Research Station, Fort Collins, CO, pp. LA1–LA51.
- Knorr, W., Jiang, L., Arneith, A., 2016. Climate, CO₂ and human population impacts on global wildfire emissions. *Biogeosciences* 13, 267.
- Kopltz, S.N., Mickley, L.J., Marlier, M.E., Buonocore, J.J., Kim, P.S., Liu, T., Sulprizio, M.P., DeFries, R.S., Jacob, D.J., Schwartz, J., Pongsi, M., Myers, S.S., 2016. Public health impacts of the severe haze in Equatorial Asia in September–October 2015: demonstration of a new framework for informing fire management strategies to reduce downwind smoke exposure. *Environ. Res. Lett.* 11, 094023.
- Koutsias, N., Karteris, M., 1998. Logistic regression modelling of multitemporal Thematic Mapper data for burned area mapping. *Int. J. Remote Sens.* 19, 3499–3514.
- Koutsias, N., Karteris, M., 2000. Burned area mapping using logistic regression modeling of a single post-fire Landsat-5 Thematic Mapper image. *Int. J. Remote Sens.* 21, 673–687.
- Koutsias, N., Karteris, M., Fernandez-Palacios, A., Navarro, C., Jurado, J., Navarro, R., Lobo, A., 1999. Burned land mapping at local scale. In: Chuvieco, E. (Ed.), *Remote Sensing of Large Wildfires in the European Mediterranean Basin*. Springer-Verlag, Berlin Heidelberg, pp. 157–187.
- Koutsias, N., Mallinis, G., Karteris, M., 2009. A forward/backward principal component analysis of Landsat-7 ETM+ data to enhance the spectral signal of burnt surfaces. *ISPRS J. Photogramm. Remote Sens.* 64, 37–46.
- Kurum, M., 2015. C-band SAR backscatter evaluation of 2008 Gallipoli Forest Fire. *IEEE Trans. Geosci. Remote Sens. Lett.* 12, 1091–1095.
- Lamarque, J.-F., Shindell, D.T., Josse, B., Young, P.J., Cionni, I., Eyring, V., Bergmann, D., Cameron-Smith, P., Collins, W.J., Doherty, R., Dalsoren, S., Faluvegi, G., Folberth, G., Ghan, S.J., Horowitz, L.W., Lee, Y.H., MacKenzie, I.A., Nagashima, T., Naik, V., Plummer, D., Righi, M., Rumbold, S.T., Schulz, M., Skeie, R.B., Stevenson, D.S., Strode, S., Sudo, K., Szopa, S., Voulgarakis, A., Zeng, G., 2013. The Atmospheric Chemistry and Climate Model Intercomparison Project (ACCMIP): overview and description of models, simulations and climate diagnostics. *Geosci. Model Dev.* 6, 179–206. <https://doi.org/10.5194/gmd-6-179-2013>.
- Landry, R., Ahern, F., O'Neil, R., 1995. Forest burn visibility on C-HH radar images. *Can. J. Remote Sens.* 21, 204–206.
- Langaas, S., 1992. Temporal and spatial distribution of Savanna fires in Senegal and the Gambia, West Africa, 1989–90, derived from multi-temporal AVHRR night images.

- Int. J. Wildland Fire 2, 21–36.
- Laris, P.S., 2005. Spatiotemporal problems with detecting and mapping mosaic fire regimes with coarse-resolution satellite data in savanna environments. *Remote Sens. Environ.* 99, 412–424.
- Laurent, P., Mouillot, F., Yue, C., Ciaï, P., Moreno, M.V., Nogueira, J.M.P., 2018. FRY, a global database of fire patch functional traits derived from space-borne burned area products. *Sci. Data* 5, 180132.
- Le Toan, T., Beaudoin, A., Guyon, D., 1992. Relating forest biomass to SAR data. *IEEE Trans. Geosci. Remote Sens.* 30, 403–411.
- Lee, B.S., Alexander, M.E., Hawkes, B.C., Lynham, T.J., Stocks, B.J., Englefield, P., 2002. Information systems in support of wildland fire management decision making in Canada. *Comput. Electron. Agric.* 37, 185–198.
- van Leeuwen, T.T., van der Werf, G.R., Hoffmann, A.A., Detmers, R.G., Rücker, G., French, N.H.F., Archibald, S., Carvalho Jr., J.A., Cook, G.D., de Groot, W.J., Hély, C., Kasischke, E.S., Kloster, S., McCarty, J.L., Pettinari, M.L., Savadogo, P., Alvarado, E.C., Boschetti, L., Manuri, S., Meyer, C.P., Siegert, F., Trollope, L.A., Trollope, W.S.W., 2014. Biomass burning fuel consumption rates: a field measurement database. *Biogeosciences* 11, 7305–7329.
- Lewis, A.J., Henderson, F.M., 1999. Radar fundamentals: the Geoscience perspective. In: Henderson, F.M., Lewis, A.J. (Eds.), *Principles and Applications of Imaging Radar*. John Wiley & Sons, pp. 866.
- Lewis, S.L., Edwards, D.P., Galbraith, D., 2015. Increasing human dominance of tropical forests. *Science* 349, 827–832.
- Libonati, R., DaCamara, C.C., Pereira, J.M.C., Peres, L.F., 2011. On a new coordinate system for improved discrimination of vegetation and burned areas using MIR/NIR information. *Remote Sens. Environ.* 115, 1464–1477.
- Liew, S.C., Kwok, L.K., Padmanabhan, K., Lim, O.K., Lim, H., 1999. Delineating land/forest fire burnt scars with ERS interferometric synthetic aperture radar. *Geophys. Res. Lett.* 26, 2409–2412.
- Lobert, J.M., Keene, W.C., Logan, J.A., Yevich, R., 1999. Global chlorine emissions from biomass burning: reactive chlorine emissions inventory. *J. Geophys. Res.-Atmos.* 104 (D7), 8373–8389.
- Lohberger, S., Stängel, M., Atwood, E.C., Siegert, F., 2018. Spatial evaluation of Indonesia's 2015 fire-affected area and estimated carbon emissions using Sentinel-1. *Glob. Chang. Biol.* 24, 644–654.
- López García, M.J., Caselles, V., 1991. Mapping burns and natural reforestation using thematic mapper data. *Geocarto Int.* 1, 31–37.
- Loveland, T.R., Dwyer, J.L., 2012. Landsat: building a strong future. *Remote Sens. Environ.* 122, 22–29.
- Mallinis, G., Mitsopoulos, I., Chrysafi, I., 2018. Evaluating and comparing Sentinel 2A and Landsat-8 Operational Land Imager (OLI) spectral indices for estimating fire severity in a Mediterranean pine ecosystem of Greece. *Sci. Remote. Sens.* 55, 1–18.
- Mangeon, S., Field, R., Fromm, M., McHugh, C., Voulgarakis, A., 2016. Satellite versus ground-based estimates of burned area: a comparison between MODIS based burned area and fire agency reports over North America in 2007. *Anthropol. Rev.* 3, 76–92.
- van Marle, M.J.E., Kloster, S., Magi, B.I., Marlon, J.R., Daniau, A.-L., Field, R.D., Armeth, A., Forrest, M., Hantson, S., Kehrwald, N.M., Knorr, W., Lasslop, G., Li, F., Mangeon, S., Yue, C., Kaiser, J.W., van der Werf, G.R., 2017. Historic global biomass burning emissions for CMIP6 (BB4CMIP) based on merging satellite observations with proxies and fire models (1750–2015). *Geosci. Model Dev.* 10, 3329–3357. <https://doi.org/10.5194/gmd-10-3329-2017>.
- Marlon, J.R., Bartlein, P.J., Daniau, A.-L., Harrison, S.P., Maezumi, S.Y., Power, M.J., Tinner, W., Vannié, B., 2013. Global biomass burning: a synthesis and review of Holocene paleofire records and their controls. *Quat. Sci. Rev.* 65, 5–25.
- Martín, M.P., Chuvieco, E., 1993. Mapping and evaluation of burned land from multi-temporal analysis of AVHRR NDVI images. In: Kennedy, P.J., Karteris, M. (Eds.), *International Workshop: Satellite Technology and GIS for Mediterranean Forest Mapping and Fire Management*, pp. 71–83 (Thessaloniki, Greece).
- Martín, M.P., Chuvieco, E., 1995. Mapping and evaluation of burned land from multi-temporal analysis of AVHRR NDVI images. *EARSeL Adv. Remote Sens.* 4 (3), 7–13.
- Martín, M.P., Chuvieco, E., 1998. Cartografía de grandes incendios forestales en la Península Ibérica a partir de imágenes NOAA-AVHRR. *Serie Geográfica* 7, 109–128.
- Martín, M.P., Gómez, I., Chuvieco, E., 2006. Burnt Area Index (BAIM) for burned area discrimination at regional scale using MODIS data. *For. Ecol. Manag.* S221.
- Matson, M., Holben, B., 1987. Satellite detection of tropical burning in Brazil. *Int. J. Remote Sens.* 8, 509–516.
- Matson, M., Schneider, S.R., Aldridge, B., Satchwell, B., 1984. Fire Detection Using the NOAA-Series Satellites. NOAA, Washington, D.C.
- Matthias, V., Arndt, J.A., Aulinger, A., Bieser, J., Denier van der Gon, H., Kranenburg, R., Kuenen, J., Neumann, D., Poulou, G., Quante, M., 2018. Modeling emissions for three-dimensional atmospheric chemistry transport models. *J. Air Waste Manag. Assoc.* 68 (8), 763–800. <https://doi.org/10.1080/10962247.2018.1424057>.
- McCarley, T.R., Kolden, C.A., Vaillant, N.M., Hudak, A.T., Smith, A.M., Kreitler, J., 2017a. Landscape-scale quantification of fire-induced change in canopy cover following mountain pine beetle outbreak and timber harvest. *For. Ecol. Manag.* 391, 164–175.
- McCarley, T.R., Kolden, C.A., Vaillant, N.M., Hudak, A.T., Smith, A.M., Wing, B.M., Kellogg, B.S., Kreitler, J., 2017b. Multi-temporal LiDAR and Landsat quantification of fire-induced changes to forest structure. *Remote Sens. Environ.* 191, 419–432.
- McWethy, D., Higuera, P., Whitlock, C., Veblen, T., Bowman, D., Cary, G., Haberle, S., Keane, R., Maxwell, B., McGlone, M., 2013. A conceptual framework for predicting temperate ecosystem sensitivity to human impacts on fire regimes. *Glob. Ecol. Biogeogr.* 22, 900–912.
- Meddens, A.J.H., Kolden, C.A., Lutz, J.A., Abatzoglou, J.T., Hudak, A.T., 2018. Spatio-temporal patterns of unburned areas within fire perimeters in the Northwestern United States from 1984 to 2014. *Ecosphere* 9 (2), e02029.
- Menges, C.H., Bartolo, R.E., Bell, D., Hill, G.J.E., 2004. The effect of savanna fires on SAR backscatter in northern Australia. *Int. J. Remote Sens.* 25, 4857–4871.
- Mieville, A., Granier, C., Lioussé, C., Guillaume, B., Mouillot, F., Lamarque, J.F., Gregoire, J.M., Petron, G., 2010. Emissions of gases and particles from biomass burning during the 20th century using satellite data and an historical reconstruction. *Atmos. Environ.* 44 (11), 1469–1477.
- Milne, A.K., 1986. The use of remote sensing in mapping and monitoring vegetational change associated with bushfire events in Eastern Australia. *Geocarto Int.* 1, 25–32.
- Mitri, G.H., Gitas, I.Z., 2010. Mapping postfire vegetation recovery using EO-1 hyperion imagery. *IEEE Geosci. Remote Sens. Lett.* 48, 1613–1618. <https://doi.org/10.1109/TGRS.2009.2031557>.
- Mohler, R.L., Goodin, D.G., 2012. Identifying a suitable combination of classification technique and bandwidth(s) for burned area mapping in tallgrass prairie with MODIS imagery. *Int. J. Appl. Earth Obs. Geoinf.* 14, 103–111. <https://doi.org/10.1016/j.jag.2011.08.008>.
- Montealegre, A., Lamelas, M., Tanase, M., de la Riva, J., 2014. Forest fire severity assessment using ALS data in a Mediterranean environment. *Remote Sens.* 6, 4240–4265.
- Moreno Ruiz, J.A., Riano, D., Arbelo, M., French, N.H., Ustin, S.L., Whiting, M.L., 2012. Burned area mapping time series in Canada (1984–1999) from NOAA-AVHRR LTDR: A comparison with other remote sensing products and fire perimeters. *Remote Sens. Environ.* 117, 407–414.
- Moreno Ruiz, J., Lázaro, J., Cano, I., Leal, P., 2014. Burned area mapping in the North American boreal forest using Terra-MODIS LTDR (2001–2011): a comparison with the MCD45A1, MCD64A1 and BA GEOLAND-2 products. *Remote Sens.* 6, 815.
- Mouillot, F., Field, C.B., 2005. Fire history reconstruction and the global carbon budget: a 1° × 1° fire reconstruction for the 20th century. *Glob. Chang. Biol.* 11 (3), 398–420.
- Mouillot, F., Narasimha, A., Balkanski, Y., Lamarque, J.F., Field, C.B., 2006. Global carbon emissions from biomass burning in the 20th century. *Geophys. Res. Lett.* 33, L01801. <https://doi.org/10.1029/2005GL024707>.
- Mouillot, F., Schultz, M.G., Yue, C., Cadule, P., Tansey, K., Ciaï, P., Chuvieco, E., 2014. Ten years of global burned area products from spaceborne remote sensing—a review: analysis of user needs and recommendations for future developments. *Int. J. Appl. Earth Obs. Geoinf.* 26, 64–79.
- Mu, M., Randerson, J.T., van der Werf, G.R., Giglio, L., Kasibhatla, P., Morton, D., Collatz, G.J., Defries, R.S., Hyer, E.J., Prins, E.M., Griffith, D.W.T., Wunch, D., Toon, G.C., Sherlock, V., Wennberg, P.O., 2011. Daily and 3-hourly variability in global fire emissions and consequences for atmospheric model predictions of carbon monoxide. *J. Geophys. Res.-Atmos.* 116, D24303. <https://doi.org/10.1029/2011JD016245>.
- Muirhead, K., Cracknell, A.P., 1985. Straw burning over Great Britain detected by AVHRR. *Int. J. Remote Sens.* 6, 827–833.
- Müller, J.-F., 1992. Geographical distribution and seasonal variation of surface emissions and deposition velocities of atmospheric trace gases. *J. Geophys. Res.* 97 (91), 3787.
- Nielsen, T.T., Mbow, C., Kane, R., 2002. A statistical methodology for burned area estimation using multitemporal AVHRR data. *Int. J. Remote Sens.* 23, 1181–1196.
- Nogueira, J., Ruffault, J., Chuvieco, E., Mouillot, F., 2017. Can we go beyond burned area in the assessment of global remote sensing products with fire patch metrics? *Remote Sens.* 9, 7.
- Nunes, M.C.S., Vasconcelos, M.J., Pereira, J.M.C., Dasgupta, N., Alldredge, R.J., 2005. Land cover type and fire in Portugal: do fires burn land cover selectively? *Landscape* 20, 661–673.
- Oliva, P., Martin, P., Chuvieco, E., 2011. Burned area mapping with MERIS post-fire image. *Int. J. Remote Sens.* 32, 4175–4201.
- Oliveira, S.L., Pereira, J.M., Carreiras, J.M., 2012. Fire frequency analysis in Portugal (1975–2005), using Landsat-based burnt area maps. *Int. J. Wildland Fire* 21, 48–60.
- Padilla, M., Stehman, S.V., Chuvieco, E., 2014. Validation of the 2008 MODIS-MCD45 global burned area product using stratified random sampling. *Remote Sens. Environ.* 144, 187–196.
- Padilla, M., Stehman, S.V., Hantson, S., Oliva, P., Alonso-Canas, I., Bradley, A., Tansey, K., Mota, B., Pereira, J.M., Chuvieco, E., 2015. Comparing the accuracies of remote sensing global burned area products using stratified random sampling and estimation. *Remote Sens. Environ.* 160, 114–121.
- Padilla, M., Olofsson, P., Stehman, S.V., Tansey, K., Chuvieco, E., 2017. Stratification and sample allocation for reference burned area data. *Remote Sens. Environ.* 203, 240–255.
- Page, S.E., Siegert, F., Rieley, J.O., Boehm, H.V., Jaya, A., Limin, S., 2002. The amount of carbon released from peat and forest fires in Indonesia during 1997. *Nature* 420, 61–65.
- Pereira, J.M.C., 1999. A comparative evaluation of NOAA-AVHRR vegetation indexes for burned surface detection and mapping. *IEEE Trans. Geosci. Remote Sens.* 37, 217–226.
- Pereira, M.C., Setzer, A.W., 1993. Spectral characteristics of deforestation fires in NOAA-AVHRR images. *Int. J. Remote Sens.* 14, 583–597.
- Pereira, J.M.C., Sa, A.C.L., Sousa, A.M.O., Silva, J.M.N., Santos, T.N., Carreiras, J.M.B., 1999. Spectral characterisation and discrimination of burnt areas. In: Chuvieco, E. (Ed.), *Remote Sensing of Large Wildfires in the European Mediterranean Basin*. Springer-Verlag, Berlin, pp. 123–138.
- Pereira, J.M.C., Mota, B., Privette, J.L., Caylor, K.K., Silva, J.M.N., Sa, A.C.L., Ni-Meister, W., 2004. A simulation analysis of the detectability of understory burns in miombo woodlands. *Remote Sens. Environ.* 93, 296–310.
- Pflugmacher, D., Cohen, W.B., Kennedy, R.E., 2012. Using Landsat-derived disturbance history (1972–2010) to predict current forest structure. *Remote Sens. Environ.* 122, 146–165.
- Pinty, B., Verstraete, M.M., 1992. GEMI: a non-linear index to monitor global vegetation from satellites. *Vegetatio* 101, 15–20.
- Pleniou, M., Koutsias, N., 2013. Sensitivity of spectral reflectance values to different burn and vegetation ratios: a multi-scale approach applied in a fire affected area. *ISPRS J.*

- Photogramm. Remote Sens. 79, 199–210.
- Plummer, S., Arino, O., Simon, M., Steffen, W., 2006. Establishing a earth observation product service for the terrestrial carbon community: the GLOBCARBON initiative. *Mittg. Adapt. Strateg. Glob. Chang.* 11, 97–111.
- Polychronaki, A., Gitas, I.Z., 2010. The development of an operational procedure for burned-area mapping using object-based classification and ASTER imagery. *Int. J. Remote Sens.* 31, 1113–1120. <https://doi.org/10.1080/01431160903334497>.
- Polychronaki, A., Gitas, I.Z., 2012. Burned area mapping in Greece using SPOT-4 HRVIR images and object-based image analysis. *Remote Sens.* 4, 424–438. <https://doi.org/10.3390/rs4020424>.
- Polychronaki, A., Gitas, I.Z., Veraverbeke, S., Debien, A., 2013. Evaluation of ALOS PALSAR imagery for burned area mapping in Greece using object-based classification. *Remote Sens.* 5, 5680–5701.
- Prins, E.M., Menzel, W.P., 1992. Geostationary satellite detection of biomass burning in South America. *Int. J. Remote Sens.* 13, 2783–2799.
- Prins, E.M., Menzel, W.P., 1994. Trends in South American biomass burning detected with the GOES visible infrared spin scan radiometer atmospheric sounder from 1983 to 1991. *J. Geophys. Res.-Atmos.* 99, 16719–16735.
- Pulliaainen, J.T., Heiska, K., Hyyappa, J., Hallikainen, M.T., 1994. Backscattering properties of boreal forests at the C- and X-Bands. *IEEE Trans. Geosci. Remote Sens.* 32, 1041–1050.
- Pyne, S.J., 1995. *World Fire. The Culture of Fire on Earth.* University of Washington Press, Seattle and London.
- Quintano, C., Fernández-Manso, A., Stein, A., Bijker, W., 2011. Estimation of area burned by forest fires in Mediterranean countries: a remote sensing data mining perspective. *For. Ecol. Manag.* 262, 1597–1607.
- Quintano, C., Fernández-Manso, A., Roberts, D.A., 2013. Multiple Endmember Spectral Mixture Analysis (MESMA) to map burn severity levels from Landsat images in Mediterranean countries. *Remote Sens. Environ.* 136, 76–88.
- Ramo, R., Chuvieco, E., 2017. Developing a random forest algorithm for MODIS global burned area classification. *Remote Sens.* 9, 1193.
- Ramo, R., García, M., Rodríguez, D., Chuvieco, E., 2018. A data mining approach for global burned area mapping. *Int. J. Appl. Earth Obs. Geoinf.* 73, 39–51.
- Randerson, J., Chen, Y., Werf, G., Rogers, B., Morton, D., 2012. Global burned area and biomass burning emissions from small fires. *J. Geophys. Res. Biogeosci.* 117, G04012, 1–23.
- Reddy, A.D., Hawbaker, T.J., Wurster, F., Zhu, Z., Ward, S., Newcomb, D., Murray, R., 2015. Quantifying soil carbon loss and uncertainty from a peatland wildfire using multi-temporal LiDAR. *Remote Sens. Environ.* 170, 306–316.
- Reid, C.E., Brauer, M., Johnston, F.H., Jerrett, M., Balmes, J.R., Elliott, C.T., 2016. Critical review of health impacts of wildfire smoke exposure. *Environ. Health Perspect.* 124, 1334.
- Ressl, R., Lopez, G., Cruz, I., Colditz, R.R., Schmidt, M., Ressler, S., Jiménez, R., 2009. Operational active fire mapping and burnt area identification applicable to Mexican Nature Protection Areas using MODIS and NOAA-AVHRR direct readout data. *Remote Sens. Environ.* 113, 1113–1126.
- Riño, D., Moreno Ruiz, J.A., Isidoro, D., Ustin, S.L., 2007. Global spatial patterns and temporal trends of burned area between 1981 and 2000 using NOAA-NASA pathfinder. *Glob. Chang. Biol.* 13, 40–50. <https://doi.org/10.1111/j.1365-2486.2006.01268>.
- Richards, J.A., 1984. Thematic mapping from multitemporal image data using the principal components transformation. *Remote Sens. Environ.* 16, 35–46.
- Rignot, E.J., Way, J., Williams, C., Viereck, L., 1994. Radar estimates of aboveground biomass in boreal forests of interior Alaska. *IEEE Trans. Geosci. Remote Sens.* 32, 1117–1124.
- Roberts, D.A., Gardner, M., Church, R., Ustin, S., Scheer, G., Green, R., 1998. Mapping chaparral in the Santa Monica Mountains using multiple endmember spectral mixture models. *Remote Sens. Environ.* 65, 267–279.
- Roos, C.I., Scott, A.C., Belcher, C.M., Chaloner, W.G., Aylen, J., Bird, R.B., Coughlan, M.R., Johnson, B.R., Johnston, F.H., McMorrow, J., 2016. Living on a flammable planet: interdisciplinary, cross-scalar and varied cultural lessons, prospects and challenges. *Philos. Trans. R. Soc. B* 371, 20150469.
- Roteta, E., Bastarrika, A., Storm, T., Chuvieco, E., 2019. Development of a Sentinel-2 burned area algorithm: generation of a small fire database for northern hemisphere tropical. *Afr. Remote Sens. Environ.* 222, 1–17.
- Roy, D.P., Boschetti, L., 2009. Southern Africa validation of the MODIS, L3JRC and GlobCarbon burned-area products. *IEEE Trans. Geosci. Remote Sens.* 47. <https://doi.org/10.1109/TGRS.2008.2009000>.
- Roy, D.P., Giglio, L., Kendall, J.D., Justice, C.O., 1999. Multi-temporal active-fire based burn scar detection algorithm. *Int. J. Remote Sens.* 20, 1031–1038.
- Roy, D., Jin, Y., Lewis, P., Justice, C., 2005. Prototyping a global algorithm for systematic fire-affected area mapping using MODIS time series data. *Remote Sens. Environ.* 97, 137–162.
- Roy, D.P., Boschetti, L., Justice, C.O., 2008. The collection 5 MODIS burned area product — global evaluation by comparison with the MODIS active fire product. *Remote Sens. Environ.* 112, 3690–3707.
- Ruecker, G., Siegert, F., 2000. Burn scar mapping and fire damage assessment using ERS-2 Sar images in East Kalimantan, Indonesia. *Int. Arch. Photogramm. Remote. Sens. Spat. Inf. Sci.* 33, 1286–1293.
- Sader, S.A., Stone, T.A., Joyce, A.T., 1990. Remote sensing of tropical forest: an overview of research and applications using non-photographic sensors. *Photogramm. Eng. Remote. Sens.* 56, 1343–1351.
- Sandberg, G., Ulander, L.M.H., Fransson, J.E.S., Holmgren, J., Toan, T.L., 2011. L- and P-band backscatter intensity for biomass retrieval in hemiboreal forest. *Remote Sens. Environ.* 115, 2874–2886.
- San-Miguel-Ayanz, J., Schulte, E., Schmuck, G., Camia, A., Strohli, P., Liberta, G., Giovando, C., Boca, R., Sedano, F., Kempeneers, P., 2012. Comprehensive monitoring of wildfires in Europe: the European forest fire information system (EFFIS). *Approaches to Managing Disaster-Assessing Hazards. Emergencies and Disaster Impacts 87–108* (Rijeka: InTech).
- Schroeder, W., Oliva, P., Giglio, L., Quayle, B., Lorenz, E., Morelli, F., 2016. Active fire detection using Landsat-8/OLI data. *Remote Sens. Environ.* 185, 210–220.
- Schroeder, T.A., Schleeuwis, K.G., Moisen, G.G., Toney, C., Cohen, W.B., Freeman, E.A., Yang, Z., Huang, C., 2017. Testing a Landsat-based approach for mapping disturbance causality in U.S. forests. *Remote Sens. Environ.* 195, 230–243. <https://doi.org/10.1016/j.rse.2017.03.033>.
- Schultz, M., Clevers, J.G., Carter, S., Verbesselt, J., Avitabile, V., Quang, H.V., Herold, M., 2016. Performance of vegetation indices from Landsat time series in deforestation monitoring. *Int. J. Appl. Earth Obs. Geoinf.* 52, 318–327.
- Seiler, W., Crutzen, P.J., 1980. Estimates of gross and net fluxes of carbon between the biosphere and the atmosphere from biomass burning. *Clim. Chang.* 2, 207–247.
- Setzer, A.W., Pereira, J.M.C., 1991. Amazonia biomass burnings in 1987 and an estimate of their tropospheric emissions. *Ambio* 20, 19–23.
- Siegert, F., Ruecker, G., 2000. Use of multitemporal ERS-2 SAR images for identification of burned scars in south-east Asian tropical rainforest. *Int. J. Remote Sens.* 21, 831–837.
- Siljeström, P., Moreno, A., 1995. Monitoring burnt areas by principal components analysis of multi-temporal TM data. *Int. J. Remote Sens.* 16, 1577–1587.
- Silva, J.M.N., Cadima, J.F.C.L., Pereira, J.M.C., Gregoire, J.M., 2004. Assessing the feasibility of a global model for multi-temporal burned area mapping using SPOT-VEGETATION data. *Int. J. Remote Sens.* 25, 4889–4913.
- Simon, M., Plummer, S., Fierens, F., Hoelzemann, J.J., Arino, O., 2004. Burnt area detection at global scale using ATSR-2: the GLOBSCAR products and their qualification. *J. Geophys. Res. - Atmos.* 109, D14S02. <https://doi.org/10.1029/2002JD003622>. (1–16).
- Smith, R.B., Woodgate, P.W., 1985. Appraisal of fire damage and inventory for timber salvage by remote sensing in mountain ash forests in Victoria. *Aust. For.* 48, 252–263.
- Storey, E.A., Stow, D.A., O'Leary, J.F., 2016. Assessing postfire recovery of chamise chaparral using multi-temporal spectral vegetation index trajectories derived from Landsat imagery. *Remote Sens. Environ.* 183, 53–64.
- Strode, S.A., Worden, H.M., Damon, M., Douglass, A.R., Duncan, B.N., Emmons, L.K., Lamarque, J.-F., Manyin, M., Oman, L.D., Rodriguez, J.M., Strahan, S.E., Tilmes, S., 2016. Interpreting space-based trends in carbon monoxide with multiple models. *Atmos. Chem. Phys.* 16, 7285–7294. <https://doi.org/10.5194/acp-16-7285-2016>.
- Stroppiana, D., Pinnock, S., Gregoire, J.M., 2000. The Global Fire Product: daily fire occurrence from April 1992 to December 1993 derived from NOAA AVHRR data. *Int. J. Remote Sens.* 21, 1279–1288.
- Stroppiana, D., Bordogna, G., Boschetti, M., Carrara, P., Boschetti, L., Brivio, P.A., 2012a. Positive and negative information for assessing and revising scores of burn evidence. *IEEE Geosci. Remote Sens. Lett.* 9, 363–367.
- Stroppiana, D., Bordogna, G., Carrara, P., Boschetti, M., Boschetti, L., Brivio, P., 2012b. A method for extracting burned areas from Landsat TM/ETM+ images by soft aggregation of multiple spectral indices and a region growing algorithm. *ISPRS J. Photogramm. Remote Sens.* 69, 88–102.
- Stroppiana, D., Azar, R., Calò, F., Pepe, A., Imperatore, P., Boschetti, M., Silva, J., Brivio, P.A., Lanari, R., 2015. Integration of optical and SAR data for burned area mapping in Mediterranean Regions. *Remote Sens.* 7, 1320–1345.
- Tanaka, S., Kimura, H., Suga, Y., 1983. Preparation of a 1:25,000 Landsat map for assessment of burnt area on Etajima Island. *Int. J. Remote Sens.* 4, 17–31.
- Tanase, M.A., Santoro, M., de la Riva, J., Perez-Cabello, F., Le Toan, T., 2010a. Sensitivity of X-, C-, and L-band SAR backscatter to burn severity in Mediterranean pine forests. *IEEE Trans. Geosci. Remote Sens.* 48, 3663–3675.
- Tanase, M.A., Santoro, M., Wegmuller, U., de la Riva, J., Perez-Cabello, F., 2010b. Properties of X-, C- and L-band repeat-pass interferometric SAR coherence in Mediterranean pine forests affected by fires. *Remote Sens. Environ.* 114, 2182–2194.
- Tanase, M.A., Santoro, M., Aponte, C., de la Riva, J., 2014. Polarimetric properties of burned forest areas at C- and L-band. *IEEE J. Sel. Top. Appl. Earth Observ. Remote Sens.* 7, 267–276.
- Tanase, M.A., Kennedy, R., Aponte, C., 2015a. Fire severity estimation from space: A comparison of active and passive sensors and their synergy for different forest types. *Int. J. Wildland Fire* 24, 1062–1075.
- Tanase, M.A., Kennedy, R., Aponte, C., 2015b. Radar Burn Ratio for fire severity estimation at canopy level: an example for temperate forests. *Remote Sens. Environ.* 170, 14–31.
- Tansey, K., Grégoire, J.M., Stroppiana, D., Sousa, A., Silva, J., Pereira, J.M., Boschetti, L., Maggi, M., Brivio, P.A., Fraser, R., Flasse, S., Ershov, D., Binaghi, E., Graetz, D., Peduzzi, P., 2004a. Vegetation burning in the year 2000: global burned area estimates from SPOT VEGETATION data. *J. Geophys. Res. - Atmos.* 109, D14S03. <https://doi.org/10.1029/2002JD003598>. (2–22).
- Tansey, K., Gregorie, J., Binaghi, E., Boschetti, L., Brivio, P.A., Ershov, D., Flasse, E., Fraser, R., Graetz, D., Maggi, M., Peduzzi, P., Pereira, J., Silva, J., Sousa, A., Stroppiana, D., 2004b. A global inventory of burned areas at 1 km. Resolution for the year 2000 derived from SPOT VEGETATION data. *Clim. Chang.* 67, 345–377.
- Tansey, K., Grégoire, J.M., Defourny, P., Leigh, R., Peckel, J.F., Bogaert, E.V., Bartholome, J.E., 2008. A new, global, multi-annual (2000–2007) burnt area product at 1 km resolution. *Geophys. Res. Lett.* 35, L01401. <https://doi.org/10.1029/2007GL03156>.
- Thonicke, K., Spessa, A., Prentice, I.C., Harrison, S.P., Dong, L., Carmona-Moreno, C., 2010. The influence of vegetation, fire spread and fire behaviour on biomass burning and trace gas emissions: results from a process-based model. *Biogeosciences* 7, 1991–2011.
- Tompoulidou, M., Stefanidou, A., Grigoriadis, D., Dragozi, E., Stavrakoudis, D., Gitas, I.Z., 2016. The Greek National Observatory of Forest Fires (NOFFI). In: Fourth

- International Conference on Remote Sensing and Geoinformation of the Environment (RSCy2016). SPIE, pp. 9688. <https://doi.org/10.1117/12.2240560>.
- Trigg, S., Flasse, S., 2000. Characterizing the spectral-temporal response of burned savannah using in situ spectroradiometry and infrared thermometry. *Int. J. Remote Sens.* 21, 3161–3168.
- Trigg, S., Flasse, S., 2001. An evaluation of different bi-spectral spaces for discriminating burned shrub-savannah. *Int. J. Remote Sens.* 22, 2641–2647.
- Vafeidis, T.A., Drake, N.A., 2005. A two-step method for estimating the extent of burnt areas with the use of coarse-resolution data. *Int. J. Remote Sens.* 26, 2441–2459.
- Vanderhoof, M.K., Brunner, N., Beal, Y.-J.G., Hawbaker, T.J., 2017a. Evaluation of the US geological survey Landsat burned area essential climate variable (BAECV) across the conterminous US using commercial high-resolution imagery. *Remote Sens.* 9, 743.
- Vanderhoof, M.K., Fairaux, N., Beal, Y.-J.G., Hawbaker, T.J., 2017b. Validation of the USGS Landsat burned area essential climate variable (BAECV) across the conterminous United States. *Remote Sens. Environ.* 198, 393–406.
- Vázquez, A., Cuevas, J.M., González-Alonso, F., 2001. Comparison of the use of WiFS and LISS images to estimate the area burned in a large forest fire. *Int. J. Remote Sens.* 22, 901–907.
- Veraverbeke, S., Hook, S.J., 2013. Evaluating spectral indices and spectral mixture analysis for assessing fire severity, combustion completeness and carbon emissions. *Int. J. Wildland Fire* 22, 707–720.
- Veraverbeke, S., Harris, S., Hook, S., 2011. Evaluating spectral indices for burned area discrimination using MODIS/ASTER (MASTER) airborne simulator data. *Remote Sens. Environ.* 115, 2702–2709.
- Veraverbeke, S., Rogers, B.M., Randerson, J.T., 2015. Daily burned area and carbon emissions from boreal fires in Alaska. *Biogeosciences* 12 (11), 3579–3601.
- Verbesselt, J., Hyndman, R., Newnham, G., Culvenor, D., 2010. Detecting trend and seasonal changes in satellite image time series. *Remote Sens. Environ.* 114, 106–115.
- Verhegghen, A., Eva, H., Ceccherini, G., Achard, F., Gond, V., Gourlet-Fleury, S., Cerutti, P.O., 2016. The potential of Sentinel satellites for burnt area mapping and monitoring in the Congo Basin forests. *Remote Sens.* 8, 986.
- Viedma, O., Melic, J., Segarra, D., Garcia-Haro, J., 1997. Modeling rates of ecosystem recovery after fires by using Landsat TM data. *Remote Sens. Environ.* 61, 383–398.
- van Wageningen, J.W., Root, R.R., Key, C.H., 2004. Comparison of AVIRIS and Landsat ETM+ detection capabilities for burn severity. *Remote Sens. Environ.* 92, 397–408.
- Wang, C., Glenn, N.F., 2009. Estimation of fire severity using pre- and post-fire LiDAR data in sagebrush steppe rangelands. *Int. J. Wildland Fire* 18, 848–856. <https://doi.org/10.1071/wf08173>.
- Ward, D.E., Hao, W.M., Susott, R.A., Babbitt, R.E., Shea, R.W., Kauffman, J.B., Justice, C.O., 1996. Effect of fuel composition on combustion efficiency and emission factors for African savanna ecosystems. *J. Geophys. Res.-Atmos.* 101, 23569–23576.
- Weih, R.C., Riggan, N.D., 2010. Object-based classification vs. pixel-based classification: comparative importance of multi-resolution imagery. *Int. Arch. Photogramm. Remote Sens. Spat. Inf. Sci.* 38, C7.
- White, J.D., Ryan, K.C., Key, C.C., Running, S.W., 1996. Remote sensing of forest fire severity and vegetation recovery. *Int. J. Wildland Fire* 6, 125–136.
- Whittier, T.R., Gray, A.N., 2016. Tree mortality based fire severity classification for forest inventories: a Pacific Northwest national forests example. *For. Ecol. Manag.* 359, 199–209.
- Wiedinmyer, C., Akagi, S.K., Yokelson, R.J., Emmons, L.K., Al-Saadi, J.A., Orlando, J.J., Soja, A.J., 2011. The Fire INventory from NCAR (FINN): a high resolution global model to estimate the emissions from open burning. *Geosci. Model Dev.* 4, 625–641. <https://doi.org/10.5194/gmd-4-625-2011>.
- Wilson, E.H., Sader, S.A., 2002. Detection of forest harvest type using multiple dates of Landsat TM imagery. *Remote Sens. Environ.* 80, 385–396.
- Wulder, M.A., White, J.C., Alvarez, F., Han, T., Rogan, J., Hawkes, B., 2009. Characterizing boreal forest wildfire with multi-temporal Landsat and LIDAR data. *Remote Sens. Environ.* 113, 1540–1555.
- Yospin, G.I., Bridgham, S.D., Neilson, R.P., Bolte, J.P., Bachelet, D.M., Gould, P.J., Harrington, C.A., Kertis, J.A., Evers, C., Johnson, B.R., 2015. A new model to simulate climate change impacts on forest succession for local land management. *Ecol. Appl.* 25 (1), 226–242.
- Yue, C., Ciais, P., Cadule, P., Thonicke, K., Archibald, S., Poulter, B., Hao, W., Hantson, S., Mouillot, F., Friedlingstein, P., 2014. Modelling the role of fires in the terrestrial carbon balance by incorporating SPITFIRE into the global vegetation model ORCHIDEE—part 1: simulating historical global burned area and fire regimes. *Geosci. Model Dev.* 7, 2747–2767.
- Yue, C., Ciais, P., Cadule, P., Thonicke, K., van Leeuwen, T.T., 2015. Modelling the role of fires in the terrestrial carbon balance by incorporating SPITFIRE into the global vegetation model ORCHIDEE – part 2: carbon emissions and the role of fires in the global carbon balance. *Geosci. Model Dev.* 8, 1285–1297.
- Zhao, F., Huang, C., Zhu, Z., 2015. Use of vegetation change tracker and support vector machine to map disturbance types in greater Yellowstone ecosystems in a 1984–2010 Landsat time series. *IEEE Geosci. Remote Sens. Lett.* 12, 1650–1654. <https://doi.org/10.1109/lgrs.2015.2418159>.
- Zhu, Z., Woodcock, C.E., 2014. Automated cloud, cloud shadow, and snow detection in multitemporal Landsat data: an algorithm designed specifically for monitoring land cover change. *Remote Sens. Environ.* 152, 217–234.